NASA CONTRACTOR REPORT

NASA CR-1817

THE EFFECTS OF NONUNIFORM SWASH-PLATE STIFFNESS ON COUPLED BLADE-CONTROL SYSTEM DYNAMICS AND STABILITY

Part I - Analysis and Application

by Vincent J. Piarulli

Prepared by
ROCHESTER APPLIED SCIENCE ASSOCIATES, INC.
Rochester, N. Y. 14618
for Langley Research Center

NATIONAL AERONAUTICS AND SPACE ADMINISTRATION • WASHINGTON, D. C. • SEPTEMBER 1971

1. Report No.	2. Government Accession No.	3. Recipient's Catalog No.
NASA CR-1817		

4. Title and Subtitle	5. Report Date
THE EFFECTS OF NONUNIFORM SWASH-PLATE STIFFNESS ON COUPLED BLADE-CONTROL SYSTEM DYNAMICS AND STABILITY PART I - ANALYSIS AND APPLICATION	September 1971 6. Performing Organization Code

7. Author(s)	8. Performing Organization Report No.
VINCENT J. PIARULLI	70-07 10. Work Unit No.

9. Performing Organization Name and Address	11. Contract or Grant No.
Rochester Applied Science Associates, Inc. 100 Allens Creek Road Rochester, New York 14618	NAS1-9496 13. Type of Report and Period Covered

12. Sponsoring Agency Name and Address	14. Sponsoring Agency Code
National Aeronautics and Space Administration Washington, D.C. 20546	Contractor Report

15. Supplementary Notes

16. Abstract

This report presents the results of a study directed at investigating the effects of an anisotropically mounted flexible swash-plate, including blade out-of-track, on the vibratory and mechanical stability characteristics of helicopter rotor systems. The analysis which has been developed is based on a combined Laplace transform and associated matrix approach. The program yields complex eigenvalues which indicate frequency and rate of growth or decay of a natural mode of the complex system. Blade modal response and swash-plate motion corresponding to a given eigenvalue are predicted. The computer program listing for this analysis is presented in Part II of this report in NASA CR 1818.

17. Key Words (Suggested by Author(s))	18. Distribution Statement
Helicopter rotor system Rotor-control system dynamics Flexible control system Coupled blade-control system dynamics	Unclassified - Unlimited

19. Security Classif. (of this report)	20. Security Classif. (of this page)	21. No. of Pages	22. Price*
Unclassified	Unclassified	81	$3.00

*For sale by the National Technical Information Service, Springfield, Virginia 22151

CONTENTS

THE EFFECTS OF NONUNIFORM SWASH-PLATE STIFFNESS ON COUPLED BLADE-CONTROL SYSTEM DYNAMICS AND STABILITY - PART I ANALYSIS AND APPLICATION*

By Vincent J. Piarulli
ROCHESTER APPLIED SCIENCE ASSOCIATES, INC.

SUMMARY

This report presents the results of a study directed at investigating the effects of an anisotropically mounted flexible swash-plate, including blade out-of-track, on the vibratory and mechanical stability characteristics of helicopter rotor systems. The analysis which has been developed is based on a combined Laplace transform and associated matrix approach. The program yields complex eigenvalues which indicate frequency and rate of growth or decay of a natural mode of the complex system. Blade modal response and swash-plate motion corresponding to a given eigenvalue are predicted.

Initial results obtained in a set of computer runs conducted at NASA, Langley under this study indicate a strong influence of the swash-plate on blade torsion and feathering modes. Using the OH-6A helicopter as a model, the program was first applied to obtain mode shapes and natural frequencies for a system of four rotor blades coupled through a swash-plate having uniform spring supports. A number of eigenvalues were found and of these there were several torsion modes that were not predicted in the single-blade analysis. The modal relationships clearly classify each of these eigenvalues as corresponding to a forward or reverse cyclic mode, an umbrella-type mode, or a reactionless mode in which the resultant forces and moments acting on the swash-plate from the blade control forces all cancel out. With uniform control stiffness, all modes except one (the reactionless mode) were found to be stable at the standard operating speed. Increased flexibility of the swash-plate tended to increase the growth rate of this instability.

Each of the modes found in the uniform case were investigated as the swash-plate support stiffnesses were made increasingly asymmetric. Reactionless and umbrella modes tended to be insensitive to this change. However, the frequencies of certain cyclic modes did change significantly, and one cyclic mode became unstable with increasing instability as the asymmetry was increased. In addition, studies done on a three-bladed rigid rotor system with a gyro stabilizer showed a strong influence of the gyro on inter-blade coupling. With respect to out-of-blade track, studies of the stability of both the three and four-bladed rotor systems showed that this effect was less significant than support asymmetry.

---

* Part II - Computer Program Listing is NASA CR-1818.

INTRODUCTION

In the dynamic analysis of a single rotor blade, one parameter which is always open to question is the effective control system stiffness. Frequently, the effective value that is used in practice is arrived at through trial and error in order to get results compatible with experiment. Furthermore, for a given blade the effective value is generally different depending on the vibration mode being investigated. Since dynamic tests of rotating blades are very difficult to perform, there is little information on full-scale experimental verification of predicted frequencies and mode shapes for rotating blades. Thus, errors in the computed coupled vibration characteristics of rotors can at most only be suspected from dynamic response data obtained in flight.

The uncertain validity of defining an effective control system stiffness for a single blade is due to the combined effects of two different situations. The first is the fact that the motions of all the blades can be coupled through the swash-plate. The second is that the instantaneous control stiffness affecting each blade of the coupled rotor system is different and can vary significantly with azimuth position. An obvious result when neither the nonuniform control stiffness nor the interblade dynamic coupling are considered is a loss of accuracy in the prediction of the vibration modes of the complete rotor system. This may result in very serious rotor blade resonance problems and the possibility of misinterpreting the cause of high oscillatory control loads in flight response data.

Interblade coupling and the presence of any nonuniformity in the torsional stiffness constraint as the azimuth position changes have significant effects on the torsional vibration characteristics of a rotating helicopter blade, especially the lower modes. To a lesser extent the periodically varying control stiffness may affect both the flapwise bending and edgewise bending if there is strong coupling between these degrees of freedom, and either the feathering or torsional degrees of freedom. Less obvious are deleterious effects which are peculiar to systems with periodically varying parameters. Regions of mechanical instability, for example, are known to be common in such systems and a periodically varying stiffness could conceivably account for subharmonic and superharmonic variations in the control loads which would be present even without aerodynamic forces.

The value of knowing the free vibration characteristics of a rotor blade system is important when it comes to minimizing the forced response arising from the aerodynamic loading. The high harmonic content of the aerodynamic forces demands an accurate representation of the modes and frequencies of the system being

excited. Recent advances in rotor aerodynamics have seen improved representations of the complex wake geometry which influences the blade air loads. If the blade aerodynamic loads programs are to be used in conjunction with the vibratory characteristics of the blades to adequately predict blade response, it may be essential to account for interblade dynamic coupling, nonuniformly varying control stiffness, as well as interblade aerodynamic coupling. The fact that this is not presently done could account for the fact that the higher harmonics of blade and control loads are not predicted very accurately.

In addition, the presence of any imbalance between rotor blades is very likely to affect the forced dynamic response and possibly the stability of a rotor system. Though the main contribution is likely to be due to interblade coupling through the hub motion, blade out-of-track may also affect the torsional degree of freedom through the mechanism of swash-plate coupling.

The purpose of this study has been the development of an analysis procedure to investigate the effects of a nonuniform swash-plate support stiffness, swash-plate flexibility, and out-of-blade track on the vibratory mechanical stability characteristics of helicopter rotor systems. With the present analysis there are no provisions for applied aerodynamic loads or for perturbation aerodynamics as a result of blade motions. Thus, all analytical results obtained are effectively those for a rotor in a vacuum. However, the analysis and programs have been developed so as to be directly useful in more extensive aeroelastic computer programs which are yet to be developed.

SYMBOLS

a_m		length of rigid rocker arm attached to $m^{\underline{th}}$ blade, meters
a_{ij}	$i,j=1,3$	elements of a 3 x 3 array of polynomials, dimensionless
$[A]$, $[\bar{A}]$		real time and Laplace transformed counterpart of the blade transfer matrix associated with a concentrated mass and inertia
$[\bar{A}]_n^k$		characteristic array for system of rotor blades coupled through control system
$[B]$		blade transfer matrix associated with a bend or finite twist

$\left[\bar{B}\right]_m^{(i)}$ matrix relating contribution to state vector at $i^{\underline{th}}$ blade station from the blade tip unknowns

$\left[\bar{b}\right]_m^{(i)}$ matrix relating contribution to state vector at $i^{\underline{th}}$ blade station from the control torque applied to blade through rocker arm

$\left[\bar{\beta}_m^k\right]$ portion of final set of rotor-swash-plate equations associated with the $m^{\underline{th}}$ blade, defined by Equation (80)

$(\bar{C}_n^{\ell})_j$ impedance associated with $j^{\underline{th}}$ spring-damper unit

c_j damper strength of $j^{\underline{th}}$ cyclic spring-damper unit supporting the swash-plate, newtons-seconds/meter

$\left[\bar{c}\right]_m^{(i)}$ matrix relating contribution to state vector at $i^{\underline{th}}$ blade station from the discontinuity in torsional deflection at the pitch bearings

$\left[\bar{c}_m^k\right]$ portion of final set of rotor-swash-plate equation coefficients associated with coupling of the $m^{\underline{th}}$ blade with the swash-plate response, defined by Equation (82)

C damper strength of collective spring-damper unit supporting swash-plate, newtons-seconds/meter

$\left[\bar{d}\right]_m^{(i)}$ matrix relating contribution to state vector at $i^{\underline{th}}$ blade station from the discontinuity in flap angle at the flap hinge

$\left[\bar{\mathcal{D}}_{nm}^k\right]$ portion of final set of rotor-swash-plate equations coefficients associated with coupling of the swash-plate response to that of the $m^{\underline{th}}$ blade, defined by Equation (79)

$\left[E\right]$, $\left[\bar{E}\right]$ real time and Laplace transformed counterpart of the blade transfer matrix associated with a massless elastic section

(EJ_z) bending stiffness of swashplate, newtons-meters^2

$\left[G\right]_m^{(i)}$, $\left[\bar{G}\right]_m^{(i)}$	transfer matrix associated with $i^{\underline{th}}$ section of $m^{\underline{th}}$ blade, real time and Laplace transformed versions, respectively
(GJ_T)	torsional stiffness of swash-plate, newtons-meters^2
i	imaginary number, $\sqrt{-1}$
k_j	stiffness of $j^{\underline{th}}$ cyclic spring-damper unit supporting swash-plate, newtons/meter
k_m	stiffness of the control rod attaching the $m^{\underline{th}}$ blade to the swash-plate, newtons/meter
K	stiffness of collective spring-damper unit supporting swash-plate, newtons/meter
$\mathcal{L}_t$	operator indicating Laplace transform with respect to time t
M_y, M_z, T	flapwise bending moment, edgewise bending moment, and torque in a rotor blade, meter-newtons
M_z	bending moment in swash-plate, meter-newtons
$(M_z)_\ell$	azimuthal harmonic of bending moment in swash-plate, meter-newtons
m	mass of swash-plate, kilograms
N_b	number of rotor blades
$N_{e.s.}$	number of concentrated supports below swash-plate
N_f	highest harmonic of periodically varying coefficients accounted for
N_{max}	highest azimuthal harmonic of swash-plate deformation accounted for
$N_{C.T.}$, N_{fea}, N_{flap}	blade station immediately inboard of which the rocker arm, pitch bearings, and flap hinge occurs, respectively

NS	number of stations or segments into which a blade is divided
$P_m(t)$, $\bar{P}_m(s)$	real time and Laplace transformed counterpart of force in control rod of $m^{\underline{th}}$ blade, newtons
$\left\{\bar{p}_n\right\}_m^{\text{blade}}$	column of blade tip unknowns and blade discontinuities
$Q(\theta,t)$	distribution of forces acting on swash-plate in a downward sense, newtons/meter
$Q_\ell(t)$	$\ell^{\underline{th}}$ azimuthal harmonic of the loading $Q(\theta,t)$
$\left\{\bar{q}_n\right\}^*$	column containing dependent variables of all blades plus swash-plate
$\left\{\bar{r}_n\right\}^{\text{swash plate}}$	column containing harmonics of swash-plate deflection
R	radius of swash-plate, meters
$\left[R\right]$	blade transfer matrix associated with a rigid massless segment - may be used for an offset in neutral axis
$\left(r_3\right)$, $\left(r_4\right)$, $\left(r_{11}\right)$	row vector having 12 elements, all of which are zero except for a value of unity in the third, fourth, and eleventh positions, respectively
s	complex number which is the Laplace transform variable corresponding to time t, radians/second
$\left\{S\right\}_m^i$, $\left\{\bar{S}\right\}_m^i$	real time and Laplace transformed version of the state vector at station i of the $m^{\underline{th}}$ blade - see Equation (35)
$\left[SK\right]$, $\left[\overline{SK}\right]$	real time and Laplace transformed version of blade transfer matrix associated with concentrated spring-damper unit.
$\left\{\bar{S}\right\}_m^{*\text{Tip}}$	modified state vector at tip of $m^{\underline{th}}$ blade, contains only nontrivial quantities
$\left[\bar{S}\right]_n^k$	portion of the final set of rotor-swash-plate equation coefficients associated with the swash-plate impedances, defined by Equation (78)

t	time, seconds
$T(\theta,t)$	torque in the swash-plate, meter-newtons
T_ℓ	azimuthal harmonic of swash-plate torque
$\left[\bar{\bar{T}}\right]^k_n$	contains coefficients for final set of equations governing swash-plate response, blade tip unknowns and blade discontinuities, defined by Equation (77)
$u_0(t)$	displacement downward of swash-plate base, meters
u_x, u_y, u_z	perturbation deflections of blade neutral axis in radial, edgewise, and flapwise senses, respectively, meters
V_y, V_z, N	edgewise shear force, flapwise shear force, and radial force in blade, respectively, newtons
V_y	transverse shear force in swash-plate, newtons
$(V_y)_\ell$	azimuthal harmonic of $V_y(\theta,t)$, newtons
$v(\theta,t)$	displacement downward of swash-plate as a function of azimuth and time (referred to fixed frame), meters
$v_\ell(t)$	azimuthal harmonic of $v(\theta,t)$
$w(\phi,t)$	displacement of swash-plate as a function of azimuth and time (referred to rotating frame), meters
$w_\ell(t)$, $\bar{w}_\ell(s)$	azimuthal harmonic of $w(\phi,t)$, real time and Laplace transformed versions, respectively (see Equation (19)
X_r, Y_r, Z_r	rectangular cartesian coordinate system rotating about X_r axis at rate of Ω radians/second
x_{rb}, y_{rb}, z_{rb}	local coordinate system attached to blade, y_{rb} directed along chord, z_{rb} normal to blade.
$\bar{X}^{k,n}_{q,\ell}$	swash-plate impedances associated with asymmetry of support configuration

$\bar{Y}^{k}_{m}$	complex function characterizing rocker arm length and control rod retardation time, meters
$\bar{Z}^{\ell}_{n}$	swash-plate impedances associated with symmetric properties of swash-plate and its support configuration
$\left[\alpha\right]$	boundary condition array on blade root displacements and slopes
δ^{i}_{j}	kronecker delta, equals unity if i=j, equals zero if $i \neq j$.
$(\overline{\Delta T})_m$, $(\overline{\Delta \phi_x})_m$, $(\overline{\Delta \phi_y})_m$	discontinuities in blade torque, torsional deflection, and flap angle of $m^{\underline{th}}$ blade
$\left\{\bar{\Delta}\right\}^{C.T.}_{m}$, $\left\{\bar{\Delta}\right\}^{fea}_{m}$, $\left\{\bar{\Delta}\right\}^{flap}_{m}$	discontinuity columns defined by Equations (46), (48) and (50), respectively
$\left\{\bar{\Delta}\right\}^{*C.T.}_{m}$, $\left\{\bar{\Delta}\right\}^{*fea}_{m}$, $\left\{\bar{\Delta}\right\}^{*flap}_{m}$	defined by Equation (55)
θ	azimuthal independent coordinate for swash-plate unknowns referred to fixed frame of reference, radians
Θ	local bending slope of elastic ring representation of swash-plate, radians
Θ_{ℓ}	azimuthal harmonic of Θ, radians
$\left[\bar{\lambda}\right]^{Tip}_{m}$	initialization array for tip unknowns, defined by Equation (41)

$\left[\bar{\lambda}\right]^{C.T.}_{m}$, $\left[\bar{\lambda}\right]^{fea}_{m}$, $\left[\bar{\lambda}\right]^{flap}_{m}$ — initialization arrays for control torque, feathering angle, and blade flap - defined by Equations (56)

μ — mass per unit arc length of swash-plate, kilograms/meter

$\pi = 3.1415927....$ — Pi

τ_m — damper time constant associated with spring-damper representation of control rod connecting $m^{\underline{th}}$ blade to swash-plate, seconds

Φ, Θ, Ψ — finite angles defining orientation of blade surface at an arbitrary radial point, Φ corresponds to forward sweep, Θ corresponds to downward coning, Ψ corresponds to nose up pretwist and/or collective angle of attack, radians

$\Phi(\theta,t)$ — swash-plate local twist slope, radians

Φ_ℓ — azimuthal harmonic of $\Phi(\theta,t)$

ϕ — azimuthal independent coordinate for swash-plate motion referred to rotating frame of reference, radians

$\phi_m = \frac{(m-1)2\pi}{N_b}$ — phase angle of $m^{\underline{th}}$ blade

ϕ_x, ϕ_y, ϕ_z — perturbation twist, flapwise bending slope, and edgewise bending slope, respectively, radians

χ_j — azimuth angle of $j^{\underline{th}}$ spring-damper unit supporting swash-plate

Ω — operating speed of rotor, radians/second

Subscripts and Superscripts:

i or (i)	superscript denoting $i^{\underline{th}}$ blade station counting inboard from tip to root, takes on values from 1 to NS
j	index
ℓ, n, p, q	indices used for harmonic number
m	index indicating $m^{\underline{th}}$ blade
+, -	used as superscripts indicate the outboard and inboard ends of a blade segment or radial station, respectively
C.T., fea, flap	used as supercripts these symbols indicate a matrix product or state vector evaluated at the control torque, pitch bearings, and flap hinges, respectively
*	used as superscript indicates a modified vector defined as in Equations (42) and (55)
$\left(\ \right)$	as in $\left(r_3\right)$ indicates a row vector
$\left[\right]$	indicates a matrix
$\left\{ \right\}$	indicates a column vector

ANALYSIS

Derivation of the Governing Equations for an Anisotropically Supported Swash-Plate

The model of the control system as shown in Figure 1 consists of: (1) a swash-plate represented by an elastic ring having uniform mass, (2) a set of spring-dampers supporting the swash-plate, (3) a single spring-damper unit in series with the first group, and (4) flexible control rods connecting the swash-plate to the rotor blades. The governing differential equations for motion of an elastic ring out of its plane consist of the following equilibrium, stress-strain, and strain-displacement equations.

$$\frac{1}{R}\frac{\partial V_y}{\partial \theta} = \mu \frac{\partial^2 v}{\partial t^2} - Q(\theta,t) \tag{1}$$

$$\frac{1}{R}\frac{\partial M_z}{\partial \theta} = - V_y - \frac{T}{R} \tag{2}$$

$$\frac{1}{R}\frac{\partial T}{\partial \theta} = \frac{M_z}{R} \tag{3}$$

$$\frac{1}{R}\frac{\partial \Theta}{\partial \theta} = - \frac{1}{R}\Phi + \frac{M_z}{(EJ_z)} \tag{4}$$

$$\frac{1}{R}\frac{\partial v}{\partial \theta} = \Theta \tag{5}$$

$$\frac{1}{R}\frac{\partial \Phi}{\partial \theta} = \frac{\Theta}{R} + \frac{T}{(GJ_T)} \tag{6}$$

where: V_y, M_z, and T are shear force, bending moment, and torque, respectively;

v is the local displacement of the swash-plate;

Θ and Φ are the local bending slope and twist angle of the ring;

R is the swash-plate radius; and

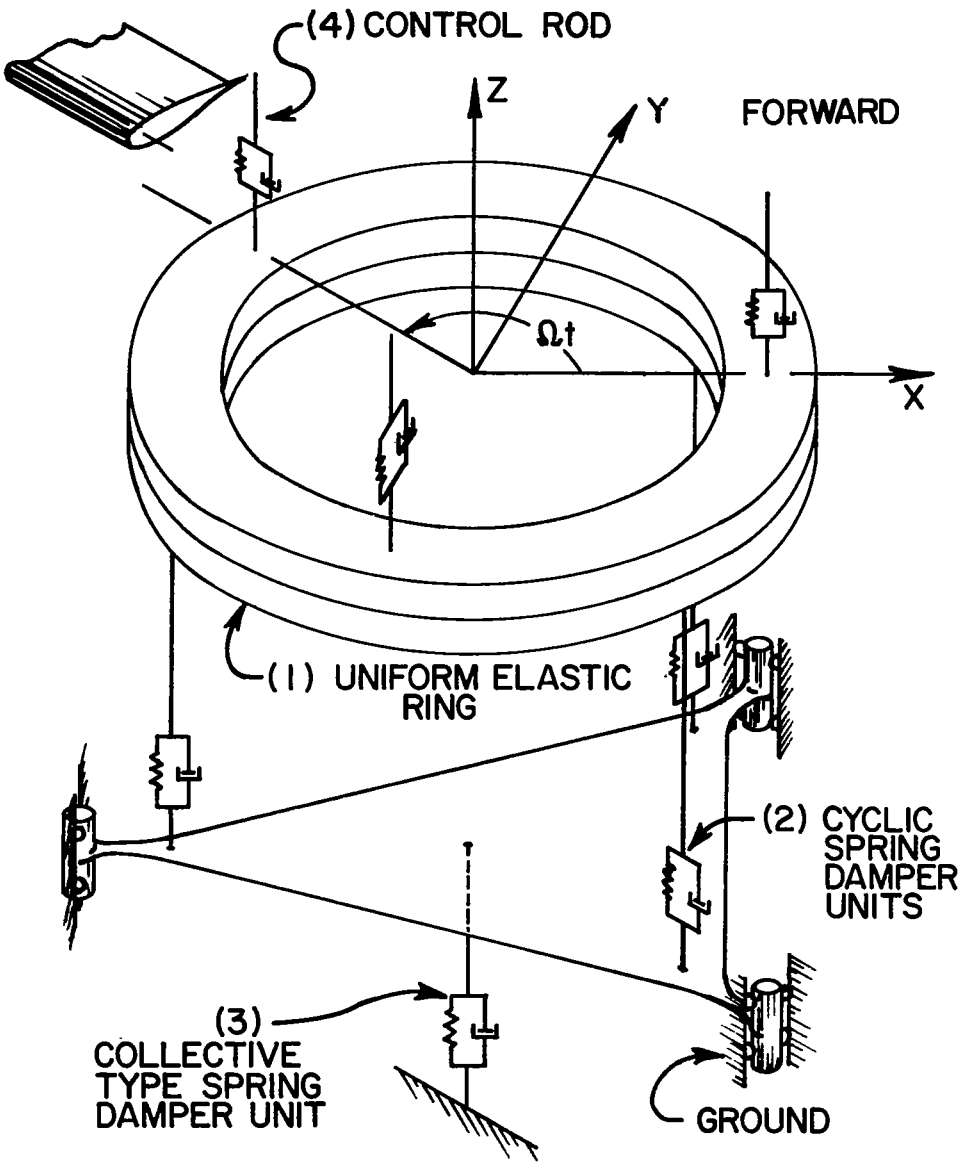

Figure 1. Model of swash-plate and support configuration

$Q(\theta,t)$ is the applied force per unit length acting on the ring.

The present model does not account for concentrated applied moments or torques applied to the swash-plate. In order to account for such effects there would have to be additional terms in Equations (2) and (3).

The orientation of each of the variables used in Equations (1) through (6) are shown in Figure 2.

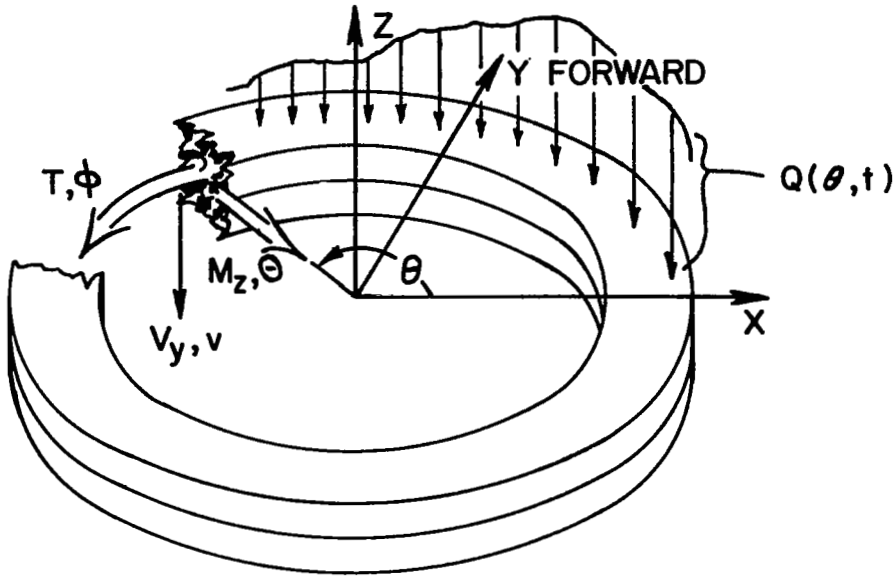

Figure 2. Coordinates of swash-plate variables

The θ dependence of the governing swash-plate partial differential equations may be removed by going to a Fourier transform. Since each of the quantities v, Φ, Θ, T, V_y, and M_z are periodic with respect to θ, each of these variables satisfies relationships of the form exemplified by $v(\theta,t)$ in the following two equations.

$$v(\theta,t) = \sum_{\ell=-\infty}^{\infty} v_\ell(t) e^{i\ell\theta} \tag{7}$$

$$v_\ell(t) = \frac{1}{2\pi} \int_0^{2\pi} v(\theta,t) e^{-i\ell\theta} \, d\theta \tag{8}$$

Thus, Equations (1) through (6) are multiplied by

$$e^{-i\ell\theta} \, d\theta$$

and the integration is performed over θ from 0 to 2π. After using the conditions of periodicity and the definitions exemplified by Equation (8) above, the following set of ordinary differential equations with time as the single independent variable are found:

$$i\ell \frac{(V_y)_\ell}{R} = \mu \frac{\partial^2 v_\ell}{\partial t^2} - Q_\ell(t) \tag{9}$$

$$i\ell \frac{(M_z)_\ell}{R} = -(V_y)_\ell - \frac{T_\ell}{R} \tag{10}$$

$$i\ell \frac{T_\ell}{R} = \frac{(M_z)_\ell}{R} \tag{11}$$

$$i\ell \frac{\Theta_\ell}{R} = -\frac{\Phi_\ell}{R} + \frac{(M_z)_\ell}{(EJ_z)} \tag{12}$$

$$i\ell \frac{v_\ell}{R} = \Theta_\ell \tag{13}$$

$$i\ell \frac{\Phi_\ell}{R} = \frac{\Theta_\ell}{R} + \frac{T_\ell}{(GJ_T)} \tag{14}$$

Equations (9) through (14) can be combined to construct the following uncoupled equation for $v_\ell(t)$ alone.

$$\mu \frac{\partial^2 v_\ell}{\partial t^2} + \frac{\ell^2}{R^4} \frac{(\ell^2-1)^2}{\left(\frac{1}{GJ_T} + \frac{\ell^2}{EJ_z}\right)} v_\ell = Q_\ell \tag{15}$$

It is interesting to note that when $\ell=0$ or ± 1 the swash-plate stiffnesses have no effect on the governing equation for v_ℓ since these are the rigid body degrees of freedom of the swash-plate. In fact, Equation (15) also indicates that as the swash-plate flexibility tends to zero, the v_ℓ must approach zero except for $\ell=0$ or ± 1.

All of the swash-plate variables used so far have been referred to a non-rotating system of coordinates. For purposes of marrying the swash-plate motion with the motion of the rotor blades it has proven to be more convenient to use swash-plate deflections measured in a rotating frame as dependent variables.

By defining

$$w(\phi,t) \triangleq v(\Omega t + \phi, t) \tag{16}$$

where Ω is the operating speed of the rotor, the quantity $w(\phi,t)$ is equal to the downward vertical displacement of the swash-plate at time t measured at an azimuth angle ϕ radians in advance of the reference blade. This assumes that the reference blade makes an angle Ωt with the x-axis as shown in Figure 1.

By means of relations (7) and (16) it can be shown that

$$v_\ell(t) = e^{-i\ell\Omega t} w_\ell(t) \tag{17}$$

where

$$w_\ell(t) = \frac{1}{2\pi} \int_0^{2\pi} w(\phi,t) e^{-i\ell\phi} \, d\phi \ . \tag{18}$$

The substitution indicated by Equation (17) can then be made in Equation (15). It should be noted that the w_ℓ's will be the dependent swash-plate unknowns from this point on and that once these quantities are found the actual swash-plate displacements

can be found from either of the following two equations:

Rotating Frame

$$w(\phi,t) = \sum_{\ell=-\infty}^{\infty} e^{i\ell\phi}\, w_\ell(t) \tag{19}$$

Non-Rotating Frame

$$v(\theta,t) = \sum_{\ell=-\infty}^{\infty} e^{i\ell(\theta-\Omega t)}\, w_\ell(t) \tag{20}$$

The following governing equation for each $w_\ell(t)$ is obtained by substituting into Equation (15) the expression for v_ℓ as given by Equation (17), and then multiplying by the factor $e^{i\ell\Omega t}$.

$$\mu\left[\frac{\partial^2 w_\ell}{\partial t^2} - 2i\ell\Omega\,\frac{\partial w_\ell}{\partial t} - \ell^2\Omega^2 w_\ell\right] + \frac{\ell^2}{R^4}\,\frac{(\ell^2-1)^2 w_\ell}{\left[\frac{1}{GJ_T} + \frac{\ell^2}{EJ_z}\right]} = Q_\ell e^{i\ell\Omega t} \tag{21}$$

Recall that $Q_\ell(t)$ was obtained from the Fourier transform of Equation (1) so that

$$Q_\ell(t) = \frac{1}{2\pi}\int_0^{2\pi} Q(\theta,t)e^{-i\ell\theta}\, d\theta \tag{22}$$

where $Q(\theta,t)$ is the applied force per unit length acting vertically downward on the elastic ring which represents the swash-plate.

One contribution to $Q(\theta,t)$ comes from the discrete forces due to the rotating control rods which couple the swash-plate with the rotor blades. The other contribution comes from the forces in the spring-damper units shown as item (2) in Figure 1.

A Dirac delta representation of the concentrated forces leads to the following expression for $Q(\theta,t)$

$$Q(\theta,t) = \sum_{m=1}^{N_b} P_m(t)\,\delta(\theta - \Omega t - \phi_m)$$

$$- \sum_{j=1}^{N_{e.s.}} \delta(\theta - \chi_j)\left(k_j + c_j \frac{\partial}{\partial t}\right)\left(v(\theta,t) - u_0(t)\right) \qquad (23)$$

where: N_b is the number of blades,

$P_m(t)$ is the force in the $m^{\underline{th}}$ control rod,

$\phi_m = \frac{(m-1)2\pi}{N_b}$ for equal spacing between control rods,

$N_{e.s.}$ is the number of spring-damper units directly supporting the swash-plate,

χ_j is the azimuthal angle locating the $j^{\underline{th}}$ support,

k_j and c_j are the stiffness and damping for the $j^{\underline{th}}$ spring damper unit,

$u_0(t)$ is the vertical downward displacement of the base which supports the spring-damper units,

and $\delta(\theta-\theta_0)$ is defined such that

$$\int_0^{2\pi} f(\theta)\,\delta(\theta - \theta_0)\,R\,d\theta = f(\theta_0) \quad . \qquad (24)$$

(θ_0 being an arbitrary azimuthal angle).

The required expression for Q_ℓ which is needed in Equation (21) is obtained by substituting the form for $Q(\theta,t)$, as given by Equation (23), into the integrand of relation (22).

Taking proper care with regard to the integral of the Dirac delta function it is found that

$$Q_\ell(t) = \frac{1}{2\pi R} \sum_{m=1}^{N_b} P_m(t) e^{-i\ell(\Omega t+\phi_m)}$$

$$- \frac{1}{2\pi R} \sum_{j=1}^{N_{e.s.}} (k_j + c_j \frac{\partial}{\partial t}) v(\chi_j,t) e^{-i\ell\chi_j}$$

$$+ \frac{1}{2\pi R} \sum_{j=1}^{N_{e.s.}} (k_j + c_j \frac{\partial}{\partial t}) u_0(t) e^{-i\ell\chi_j} \qquad (25)$$

A consideration of the equilibrium of the base supporting the spring-damper units leads to the following equation which relates $u_0(t)$ to the displacement of the swash-plate

$$(K + C \frac{\partial}{\partial t}) u_0 = \sum_{j=1}^{N_{e.s.}} (k_j + c_j \frac{\partial}{\partial t})(v(\chi_j,t) - u_0) \qquad (26)$$

In addition if use is made of the fact that

$$v(\chi_j,t) = \sum_{\ell=-\infty}^{\infty} w_\ell e^{i\ell(\chi_j-\Omega t)} \qquad (27)$$

then $Q_\ell(t)$ may be related to all the w_ℓ's and u_0; and u_0 may be related to the w_ℓ's by virtue of Equations (25), (26) and (27). The complete elimination of $u_0(t)$ as an unknown is more easily made after the following step in which the Laplace transform is taken of Equations (21), (25), and (26).

The Laplace transformed version of Equation (21) with quiescent initial conditions is given by

$$\left\{\mu[s^2 - 2i\ell\Omega s - \ell^2\Omega^2] + \frac{\ell^2(\ell^2-1)^2}{R^4\left(\frac{1}{GJ_T} + \frac{\ell^2}{EJ_z}\right)}\right\}\bar{w}_\ell(s) = L_t\left\{Q_\ell(t)e^{i\ell\Omega t}\right\} \quad (28)$$

where the standard formalism for Laplace transforms is being adhered to. That is, the Laplace transform of $w_\ell(t)$, for example, is defined as follows:

$$\bar{w}_\ell(s) \triangleq L_t\{w_\ell(t)\} \triangleq \int_0^\infty e^{-st}w_\ell(t)\,dt \quad (29)$$

From Equations (25) and (27) it may be shown that

$$L_t\left\{Q_\ell(t)e^{i\ell\Omega t}\right\} = \frac{1}{2\pi R}\sum_{m=1}^{N_b}\bar{P}_m(s)e^{-i\ell\phi_m}$$

$$- \frac{1}{2\pi R}\sum_{p=-\infty}^{\infty}\sum_{j=1}^{N_{e.s.}}[k_j + (s - i\ell\Omega)c_j]\bar{w}_p(s - i\ell\Omega + ip\Omega)e^{-i\chi_j(\ell-p)}$$

$$+ \frac{1}{2\pi R}\sum_{j=1}^{N_{e.s.}}[k_j + (s - i\ell\Omega)c_j]\bar{u}_0(s - i\ell\Omega)e^{-i\ell\chi_j} \quad (30)$$

In the last operation use has been made of a fundamental Laplace transform identity which states that

$$L_t\{f(t)e^{at}\} = \bar{f}(s - a) \quad (31)$$

It is important to realize that the quantity $\bar{w}_p(s - i\ell\Omega + ip\Omega)$ which appears in Equation (30) is not to be interpreted as a product but as a shifted argument. On the other hand, the quantity $(s - i\ell\Omega)c_j$ is simply a product.

The Laplace transformed version of Equation (26) makes it convenient to solve for $\bar{u}_0(s)$ as follows:

$$\bar{u}_0(s) = \frac{\sum_{p=-\infty}^{\infty} \sum_{j=1}^{N_{e.s.}} (k_j + sc_j) e^{ip\chi_j} \bar{w}_p(s + ip\Omega)}{K + Cs + \sum_{j=1}^{N_{e.s.}} (k_j + sc_j)} \tag{32}$$

The expression for $\bar{u}_0(s - i\ell\Omega)$ which is needed in Equation (30) may be obtained from the last equation by formally replacing s by the quantity $(s - i\ell\Omega)$.

When this has been done, the resulting expression for $\bar{u}_0(s - i\ell\Omega)$ can be substituted into expression (30) which in turn can replace the right-hand side of Equation (28). The result is the following system of coupled equations for the Laplace transformed versions of the swash-plate unknowns (the $\bar{w}_q$'s) in terms of the transform of the control rod forces ($\bar{P}_m(s)$).

$$\left[m(s^2 - 2iq\Omega s - q^2\Omega^2) + \frac{2\pi}{R^3} \frac{q^2(q^2-1)^2}{\left(\frac{1}{GJ_T} + \frac{q^2}{EJ_z}\right)} \right] \bar{w}_q(s)$$

$$+ \sum_{\ell=-\infty}^{\infty} \sum_{j=1}^{N_{e.s.}} [k_j + (s - iq\Omega)c_j] e^{-i\chi_j(q-\ell)} \bar{w}_\ell(s - iq\Omega + i\ell\Omega)$$

$$- \left\{ \sum_{\ell=-\infty}^{\infty} \frac{\left[\sum_{j=1}^{N_{e.s.}} [k_j + (s-iq\Omega)c_j] e^{-iq\chi_j}\right] \left[\sum_{j=1}^{N_{e.s.}} [k_j + (s-iq\Omega)c_j] e^{i\ell\chi_j}\right]}{K + (s-iq\Omega)C + \sum_{j=1}^{N_{e.s.}} [k_j + (s-iq\Omega)c_j]} \right\}$$

$$\cdot \left[\bar{w}_\ell(s - iq\Omega + i\ell\Omega)\right] = \sum_{m=1}^{N_b} \bar{P}_m(s) e^{-iq\phi_m} \qquad q = 0, \pm 1, \pm 2 \ldots N_{max} \tag{33}$$

where: m is the mass of the swash-plate and is equal to $2\pi R\mu$. The indices ℓ and p which have appeared in the last few equations have been replaced by q and ℓ respectively for convenience in later use.

When the governing matrix equations for the rotor blades are developed in the next section it will be the control rod forces ($P_m(s)$) which couple the swash-plate equations to the blade equations. The relation expressed by Equation (33) is the objective of this section of the report. A later section, which develops the final complete set of equations for the control system-coupled rotor blade system, begins with this relationship.

Representation of Rotor Blades By Transfer Matrices

In the transfer matrix approach used in this study, each blade is built up separately from a specified number of basic sections. Each section may be considered to have concentrated mass and inertia, uniform elastic properties, and specified geometric characteristics such as offsets and localized twist and precone.

A transfer matrix may be developed which relates a state vector at either end of a given section as follows:

$$\left\{S\right\}_m^{i-} = \left[G\right]_m^{(i)} \left\{S\right\}_m^{i+} \tag{34}$$

The state vector denoted above by $\left\{S\right\}$ is a column of twelve quantities as expressed below:

$$\left\{S\right\} = \left\{u_x \; N \; \phi_x \; T \; u_y \; \phi_z \; M_z \; -V_y \; -u_z \; \phi_y \; M_y \; V_z\right\}$$

where: u_x, u_y, u_z are displacements in the blade local x, y, and z directions,

N, V_y, V_z are axial force, edgewise shear force, and flapwise shear force, respectively,

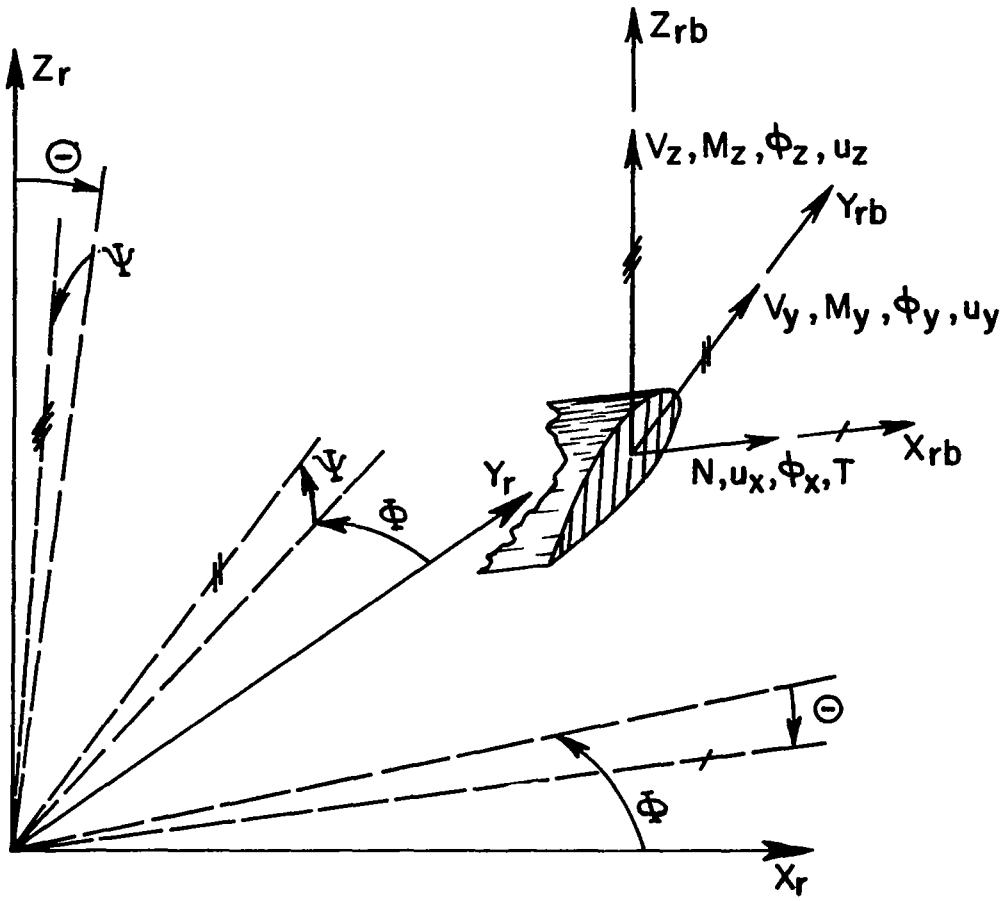

Figure 3. Blade local coordinate system and state variable orientation, slash marks refer to X, Y, and Z blade coordinates respectively

ϕ_x, ϕ_y, ϕ_z are local torsional deflection, flapwise bending slope, and edgewise bending slope, respectively

T, M_y, M_z are local torque, flapwise bending moment, and edgewise bending moment, respectively.

The local coordinate system and sense of each of the state variables is shown in Figure 3.

Referring back to Equation (34) the index i denotes the $i^{\underline{th}}$ blade section counting inboard from the blade tip. The + and - signs refer respectively to the outboard and inboard ends of the $i^{\underline{th}}$ section. The index m refers to the $m^{\underline{th}}$ blade.

In general the transfer matrix is a 12 x 12 array of differential operators, when each of the state variables is a real-time quantity. By taking the Laplace transform of Equation (34) the differential equations are converted to complex linear algebraic equations. If quiescent initial conditions are assumed, the transformed version of the transfer matrix equation for a basic section is given by

$$\left\{\bar{S}\right\}_m^{i-} = \left[\bar{G}\right]_m^{(i)} \left\{\bar{S}\right\}_m^{i+} \tag{35}$$

In practice the program does not construct the matrix $\left[G\right]_m^{(i)}$ directly but instead constructs more fundamental transfer matrices which are associated with mass, elastic, and geometric properties individually.

In the most general situation allowed for, a blade section is constructed as illustrated in Figure 4.

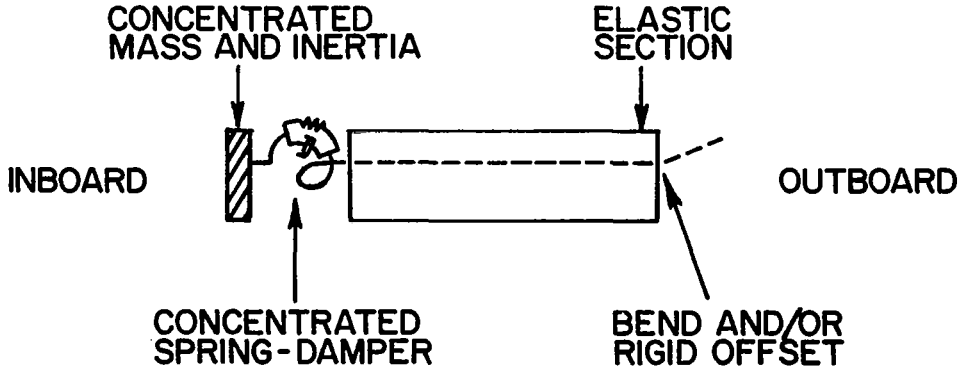

Figure 4. General blade section

A separate transfer matrix can be constructed as listed below:

$[R]$	rigid offset in the elastic axis or translation of local coordinate system
$[B]$	bend in elastic axis or more generally a rotation of local coordinates
$[E]$	uniform elastic section with centrifugal stiffness terms in addition to bending and torsional stiffnesses
$[SK]$	concentrated spring-damper (used normally for lead-lag hinge only)
$[A]$	concentrated mass and inertias

If the Laplace transform of each of the separate transfers is considered individually it can then be shown that

$$\left[\bar{G}\right]_m^{(i)} = \left[\bar{A}\right]_m^{(i)} \left[\overline{SK}\right]_m^{(i)} \left[\bar{E}\right]_m^{(i)} \left[B\right]_m^{(i)} \left[R\right]_m^{(i)} \tag{36}$$

In practice the computer program developed only constructs those matrices that are going to be needed. For example, in the case of a uniform, untwisted blade, only the mass matrices and elastic matrices would ever be constructed.

In order to develop the chain of transfer across a blade, consider the transfer across the $(i+1)^{\underline{th}}$ section

$$\left\{\bar{S}\right\}_m^{(i+1)-} = \left[\bar{G}\right]_m^{(i+1)} \left\{\bar{S}\right\}_m^{(i+1)+} \tag{37}$$

Now

$$\left\{\bar{S}\right\}^{(i+1)+} = \left\{\bar{S}\right\}^{(i)-} \tag{38}$$

Therefore, the combination of Equations (35) and (37) yields

$$\left\{\bar{S}\right\}_m^{(i+1)-} = \left[\bar{G}\right]_m^{(i+1)} \left[\bar{G}\right]_m^{(i)} \left\{\bar{S}\right\}_m^{i+} \tag{39}$$

Generalized, this collapsing procedure leads to the following expression which relates the state vector at the inboard end of the $i^{\underline{th}}$ section to the state vector at the blade tip.

$$\left\{\bar{S}\right\}^{i-} = \left[\bar{G}\right]_m^{(i)} \left[\bar{G}\right]_m^{(i-1)} \left[\bar{G}\right]_m^{(i-2)} \cdots \left[\bar{G}\right]_m^{(2)} \left[\bar{G}\right]_m^{(1)} \left\{\bar{S}\right\}_m^{Tip} \tag{40}$$

The state vector at the blade tip, which is denoted by $\left\{\bar{S}\right\}_m^{Tip}$, has six zeros due to the free boundary condition. It is very convenient to make use of this fact in the blade transfer process. It is also desirable to introduce $\bar{\lambda}$ type quantities which may be regarded as approximations to the non-zero tip unknowns in addition to new ε type unknowns which are corrections to the trial tip unknowns. It turns out that this procedure has a very beneficial effect on the accuracy of the final results. This fact which evidently was first proved in Reference (1) has manifested itself throughout the development of the computer program. The tip state vector is therefore written as follows:

$$\begin{Bmatrix} u_x \\ N \\ \phi_x \\ T \\ u_y \\ \phi_z \\ M_z \\ -V_y \\ -u_z \\ \phi_y \\ M_y \\ V_z \end{Bmatrix}_m^{Tip} = \begin{bmatrix} \bar{\lambda}_{u_x} & 1 & 0 & 0 & 0 & 0 & 0 \\ 0 & 0 & 0 & 0 & 0 & 0 & 0 \\ \bar{\lambda}_{\phi_x} & 0 & 1 & 0 & 0 & 0 & 0 \\ 0 & 0 & 0 & 0 & 0 & 0 & 0 \\ \bar{\lambda}_{u_y} & 0 & 0 & 1 & 0 & 0 & 0 \\ \bar{\lambda}_{\phi_z} & 0 & 0 & 0 & 1 & 0 & 0 \\ 0 & 0 & 0 & 0 & 0 & 0 & 0 \\ 0 & 0 & 0 & 0 & 0 & 0 & 0 \\ \bar{\lambda}_{-u_z} & 0 & 0 & 0 & 0 & 1 & 0 \\ \bar{\lambda}_{\phi_y} & 0 & 0 & 0 & 0 & 0 & 1 \\ 0 & 0 & 0 & 0 & 0 & 0 & 0 \\ 0 & 0 & 0 & 0 & 0 & 0 & 0 \end{bmatrix}_m \begin{Bmatrix} 1 \\ \bar{\varepsilon}_{ux} \\ \bar{\varepsilon}_{\phi x} \\ \bar{\varepsilon}_{uy} \\ \bar{\varepsilon}_{\phi z} \\ \bar{\varepsilon}_{-uz} \\ \bar{\varepsilon}_{\phi y} \end{Bmatrix}_m \tag{41}$$

For purposes of brevity this matrix equation will be written as follows:

$$\left\{\bar{S}\right\}_m^{Tip} = \left[\bar{\lambda}\right]_m^{Tip}\left\{\bar{S}\right\}_m^{*Tip} \tag{42}$$

The reasons for writing Equation (41) in the form shown are intimately connected with the modified transfer matrix procedure used to solve the final system of equations for the eigenvalues and eigenvectors.

The fact that the $\left[\bar{\lambda}\right]_m^{Tip}$ matrix is a 12 x 7 instead of a 12 x 12 reduces the number of computations required to obtain the transfer matrix for the whole rotor blade. This point will become more evident shortly.

Substitution of the expression for the blade tip unknowns, as given by Equation (42), into Equation (40) yields

$$\left\{\bar{S}\right\}^{i-} = \left[\bar{B}\right]_m^{(i)}\left\{\bar{S}\right\}_m^{*Tip} \tag{43}$$

where:

$$\left[\bar{B}\right]_m^{(i)} \triangleq \left[\bar{G}\right]_m^{(i)}\left[\bar{G}\right]_m^{(i-1)} \cdots \left[\bar{G}\right]_m^{(i)}\left[\bar{\lambda}\right]_m^{Tip} \tag{44}$$

The last expression is computed in practice from right to left so that the fact that $\left[\lambda\right]_m^{Tip}$ only has seven columns may be put to greatest advantage.

The transfer matrix Equation (43) holds for any station outboard of the flap hinge, pitch bearings, or a rocker arm attachment point. At these points there are discontinuities in the flap angle, torsional deflection, and blade torque, respectively.

In transferring across the rocker arm attachment point it is assumed that only the torque applied to the blade from the control system is significant. Thus the transfer inboard across the control torque point can be written as

$$\left\{\bar{S}\right\}_m^{C.T.-} = \left\{\bar{S}\right\}_m^{C.T.+} - \left\{\bar{\Delta}\right\}_m^{C.T} \tag{45}$$

where

$$\left\{\bar{\Delta}\right\}_m^{C.T.} = \left\{0\ 0\ 0\ \Delta\bar{T}\ 0\ 0\ 0\ 0\ 0\ 0\ 0\ 0\right\} \tag{46}$$

The transfer inboard across the pitch bearings is written as

$$\left\{\bar{S}\right\}_m^{fea-} = \left\{\bar{S}\right\}_m^{fea+} - \left\{\bar{\Delta}\right\}_m^{fea} \tag{47}$$

where

$$\left\{\bar{\Delta}\right\}^{fea} = \left\{0\ 0\ \overline{\Delta\phi}_x\ 0\ 0\ 0\ 0\ 0\ 0\ 0\ 0\right\} \tag{48}$$

Finally, the transfer inboard across the flap hinge, if present, is given by

$$\left\{\bar{S}\right\}_m^{flap-} = \left\{\bar{S}\right\}_m^{flap+} - \left\{\bar{\Delta}\right\}_m^{flap} \tag{49}$$

where

$$\left\{\bar{\Delta}\right\}_m^{flap} = \left\{0\ 0\ 0\ 0\ 0\ 0\ 0\ 0\ 0\ \overline{\Delta\phi}_y\ 0\ 0\right\} \tag{50}$$

Each of the quantities $\overline{\Delta T}$, $\overline{\Delta\phi}_x$, and $\overline{\Delta\phi}_y$ are additional unknowns which are to be solved for in the final system of equations. In keeping with the procedure used for the blade tip unknowns, new $\bar{\lambda}$ and $\bar{\varepsilon}$ type quantities are introduced such that:

$$
\begin{aligned}
(\Delta\bar{T})_m &= (\bar{\lambda}_{\Delta T})_m + (\bar{\varepsilon}_{\Delta T})_m \\
(\overline{\Delta\phi_x})_m &= (\bar{\lambda}_{\Delta\phi_x})_m + (\bar{\varepsilon}_{\Delta\phi_x})_m \\
(\overline{\Delta\phi_y})_m &= (\bar{\lambda}_{\Delta\phi_y})_m + (\bar{\varepsilon}_{\Delta\phi_y})_m
\end{aligned}
\tag{51}
$$

Equations (45), (47), and (49) can then be replaced by

$$
\left\{\bar{S}\right\}_m^{C.T.-} = \left\{\bar{S}\right\}_m^{C.T.+} - \left[\bar{\lambda}\right]_m^{C.T.}\left\{\bar{\Delta}\right\}_m^{*C.T.} \tag{52}
$$

$$
\left\{\bar{S}\right\}_m^{fea-} = \left\{\bar{S}\right\}_m^{fea+} - \left[\bar{\lambda}\right]_m^{fea}\left\{\bar{\Delta}\right\}_m^{*fea} \tag{53}
$$

$$
\left\{\bar{S}\right\}_m^{flap-} = \left\{\bar{S}\right\}_m^{flap+} - \left[\bar{\lambda}\right]_m^{flap}\left\{\bar{\Delta}\right\}_m^{*flap} \tag{54}
$$

where

$$
\left\{\bar{\Delta}\right\}_m^{*C.T.} \triangleq \begin{Bmatrix} 1 \\ \varepsilon_{\Delta T} \end{Bmatrix}_m ; \quad \left\{\bar{\Delta}\right\}_m^{*fea} \triangleq \begin{Bmatrix} 1 \\ \varepsilon_{\Delta\phi_x} \end{Bmatrix}_m ; \quad \left\{\bar{\Delta}\right\}_m^{*flap} \triangleq \begin{Bmatrix} 1 \\ \varepsilon_{\Delta\phi_y} \end{Bmatrix}_m \tag{55}
$$

and

$$
\left[\bar{\lambda}\right]_m^{C.T.} = \begin{bmatrix} 0 & 0 \\ 0 & 0 \\ 0 & 0 \\ \bar{\lambda}_{\Delta T} & 1 \\ 0 & 0 \\ 0 & 0 \\ 0 & 0 \\ 0 & 0 \\ 0 & 0 \\ 0 & 0 \\ 0 & 0 \\ 0 & 0 \end{bmatrix}_m ; \quad \left[\bar{\lambda}\right]_m^{fea} = \begin{bmatrix} 0 & 0 \\ 0 & 0 \\ \bar{\lambda}_{\Delta\phi_x} & 1 \\ 0 & 0 \\ 0 & 0 \\ 0 & 0 \\ 0 & 0 \\ 0 & 0 \\ 0 & 0 \\ 0 & 0 \\ 0 & 0 \\ 0 & 0 \end{bmatrix}_m ; \quad \left[\bar{\lambda}\right]_m^{flap} = \begin{bmatrix} 0 & 0 \\ 0 & 0 \\ 0 & 0 \\ 0 & 0 \\ 0 & 0 \\ 0 & 0 \\ 0 & 0 \\ 0 & 0 \\ 0 & 0 \\ \lambda_{\Delta\phi_y} & 1 \\ 0 & 0 \\ 0 & 0 \end{bmatrix}_m \tag{56}
$$

Expression (43) can now be replaced by the following matrix equation which provides the state vector at the inboard end of an arbitrary blade section

$$\left\{\bar{S}\right\}_m^{(i)} = \left[\bar{B}\right]_m^{(i)}\left\{\bar{S}\right\}_m^{*Tip} - \left[\bar{b}\right]_m^{(i)}\left\{\bar{\Delta}\right\}_m^{*C.T.} - \left[\bar{c}\right]^{(i)}\left\{\bar{\Delta}\right\}^{*fea} - \left[\bar{d}\right]^{(i)}\left\{\bar{\Delta}\right\}^{*flap} \qquad (57)$$

where by letting $N_{C.T.}$, N_{fea}, and N_{flap} be the blade section numbers immediately inboard of which the control torque, pitch bearings, and flap hinge are respectively located, the new matrices appearing in Equation (57) are given as follows:

$$\left[\bar{b}\right]_m^{(i)} \triangleq \left[\bar{G}\right]_m^{(k)}\left[\bar{G}\right]_m^{(i-1)}\cdots\left[\bar{G}\right]_m^{(N_{C.T.}+1)}\left[\bar{\lambda}\right]_m^{C.T.} \qquad i > N_{C.T.}$$

$$\triangleq \left[\bar{\lambda}\right]_m^{C.T.} \qquad i = N_{C.T.}$$

$$\triangleq \left[0\right] \qquad i < N_{C.T.} \qquad (58)$$

$$\left[\bar{c}\right]_m^{(i)} \triangleq \left[\bar{G}\right]_m^{(i)}\left[\bar{G}\right]_m^{(i-1)}\cdots\left[\bar{G}\right]_m^{(N_{fea}+1)}\left[\bar{\lambda}\right]_m^{fea} \qquad i > N_{fea}$$

$$\triangleq \left[\bar{\lambda}\right]_m^{fea} \qquad i = N_{fea}$$

$$\triangleq \left[0\right] \qquad i < N_{fea} \qquad (59)$$

$$\left[\bar{d}\right]_m^{(i)} \triangleq \left[\bar{G}\right]_m^{(i)}\left[\bar{G}\right]_m^{(i-1)} \cdots \left[\bar{G}\right]_m^{(N_{flap}+1)}\left[\bar{\lambda}\right]_m^{flap} \qquad i > N_{flap}$$

$$\triangleq \left[\bar{\lambda}\right]_m^{flap} \qquad i = N_{flap}$$

$$\triangleq \left[0\right] \qquad i < N_{flap} \qquad (60)$$

With the above definitions the state vector $\left\{\bar{S}\right\}_m^{(i)}$ when evaluated at i equal to $N_{C.T.}$, N_{fea}, or N_{flap} will be immediately inboard of the control torque point, the pitch bearings or the flap hinge, respectively.

Letting NS be the number of blade sections, the state vector at the blade root is determined from Equation (57) by letting i equal NS. If the boundary conditions at the root of each blade are such that all displacements and slopes vanish, then these conditions are expressed by the matrix equation

$$\left[\alpha\right]\left\{\bar{S}\right\}_m^{(NS)} = \left\{0\right\} \qquad (61)$$

Or, from Equation (57)

$$\left[\alpha\right]\left[\bar{B}\right]_m^{(NS)}\left\{\bar{S}\right\}_m^{*Tip} - \left[\alpha\right]\left[\bar{b}\right]_m^{(NS)}\left\{\bar{\Delta}\right\}_m^{*C.T.}$$

$$- \left[\alpha\right]\left[\bar{c}\right]_m^{(i)}\left\{\bar{\Delta}\right\}_m^{*fea} - \left[\alpha\right]\left[\bar{d}\right]_m^{(i)}\left\{\bar{\Delta}\right\}_m^{*flap} = \left\{0\right\} \qquad (62)$$

where:

$$\left[\alpha\right] \triangleq \begin{pmatrix} 1 & 0 & 0 & 0 & 0 & 0 & 0 & 0 & 0 & 0 & 0 & 0 \\ 0 & 0 & 1 & 0 & 0 & 0 & 0 & 0 & 0 & 0 & 0 & 0 \\ 0 & 0 & 0 & 0 & 1 & 0 & 0 & 0 & 0 & 0 & 0 & 0 \\ 0 & 0 & 0 & 0 & 0 & 1 & 0 & 0 & 0 & 0 & 0 & 0 \\ 0 & 0 & 0 & 0 & 0 & 0 & 0 & 0 & 1 & 0 & 0 & 0 \\ 0 & 0 & 0 & 0 & 0 & 0 & 0 & 0 & 0 & 1 & 0 & 0 \end{pmatrix} \tag{63}$$

Equation (62) provides six equations for each blade. However, there are nine possible unknowns due to the control torque, feather, and flap discontinuities. The other three equations are obtained from the condition of zero bending moment and torque at the flap hinges and pitch bearings respectively, in addition to the relationship between the control torque and the blade torsional deflection at the rocker arm attachment point.

Consider first the condition of zero torque at the blade pitch bearings. The state vector at the pitch bearings is given by $\left\{\bar{S}\right\}_m^{(N_{fea})}$. In order for the torque (which is the fourth quantity in the state vector) to vanish the following equation must be satisfied.

$$\left(r_4\right)\left\{\bar{S}\right\}_m^{(N_{fea})} = 0 \tag{64}$$

Or equivalently,

$$\left(r_4\right)\left[\bar{B}\right]_m^{(N_{fea})}\left\{\bar{S}\right\}_m^{*Tip} - \left(r_4\right)\left[\bar{b}\right]_m^{(N_{fea})}\left\{\bar{\Delta}\right\}_m^{*C.T.}$$

$$- \left(r_4\right)\left[\bar{d}\right]_m^{(N_{fea})}\left\{\bar{\Delta}\right\}^{*flap} = 0 \tag{65}$$

where $\left(r_4\right) \triangleq (0\ 0\ 0\ 1\ 0\ 0\ 0\ 0\ 0\ 0\ 0\ 0)$

The equation for the control torque must reflect the coupling between the blade and the swash-plate motion. In real time the balance of forces on the $m^{\underline{th}}$ control rod which connects the rocker arm to the swash-plate is given by

$$(\Delta T)_m = a_m k_m (1 + \tau_m \frac{\partial}{\partial t}) \left[a_m \phi_{x_m}^{N_{C.T.}} - \sum_{\ell=-\infty}^{\infty} w_\ell(t) e^{i\ell\phi_m} \right] \tag{66}$$

Dividing by k_m and taking the Laplace transform yields

$$k_m^{-1} (\Delta \bar{T})_m - a_m^2 (1 + \tau_m s) (\bar{\phi}_x)_m^{(N_{C.T.})} + \sum_{\ell=-\infty}^{\infty} a_m (1 + \tau_m s) e^{i\ell\phi_m} \bar{w}_\ell(s) = 0 \tag{67}$$

Referring to equations (51), (55), and (56) it follows that

$$(\Delta \bar{T})_m = \left(r_4\right) \left[\bar{\lambda}\right]_m^{C.T.} \left\{\bar{\Delta}\right\}_m^{*C.T.} \tag{68}$$

and

$$(\bar{\phi}_x)_m^{N_{C.T.}} = \left(r_3\right) \left\{\bar{S}\right\}_m^{(N_{C.T.})} = \left(r_3\right) \left[\bar{B}\right]_m^{(N_{C.T.})} \left\{\bar{S}\right\}_m^{*Tip} - \left(r_3\right) \left[\bar{d}\right]_m^{(N_{C.T.})} \left\{\bar{\Delta}\right\}^{*flap} \tag{69}$$

where $\left(r_3\right) = (0\ 0\ 1\ 0\ 0\ 0\ 0\ 0\ 0\ 0\ 0\ 0)$

Thus, the control torque equation can be written in terms of the blade tip and internal discontinuity unknowns as follows:

$$- a_m^2(1 + \tau_m s)\left(r_3\right)\left[\bar{B}\right]^{(N_{C.T.})}\left\{\bar{S}\right\}_m^{*Tip} + k_m^{-1}\left(r_4\right)\left[\bar{\lambda}\right]_m^{C.T.}\left\{\bar{\Delta}\right\}_m^{*C.T.}$$

$$+ a_m^2(1 + \tau_m s)\left(r_3\right)\left[\bar{d}\right]_m^{(N_{C.T.})}\left\{\bar{\Delta}\right\}^{*flap}$$

$$+ \sum_{\ell=-\infty}^{\infty} a_m(1 + \tau_m s)e^{i\ell\phi_m}\bar{w}_\ell(s) = 0 \qquad (70)$$

Finally, if a flap hinge is present the condition that the flapwise moment vanish gives the last equation needed. Since the flapwise moment is the eleventh quantity in the state vector, this condition is satisfied provided

$$\left(r_{11}\right)\left\{\bar{S}\right\}_m^{(N_{flap})} = 0 \qquad (71)$$

where $\left(r_{11}\right) \triangleq (0\ 0\ 0\ 0\ 0\ 0\ 0\ 0\ 0\ 0\ 1\ 0)$

Referring back to Equation (57), the zero flap hinge moment is expressed by

$$\left(r_{11}\right)\left[\bar{B}\right]_m^{(N_{flap})}\left\{\bar{S}\right\}_m^{*Tip} - \left(r_{11}\right)\left[\bar{b}\right]_m^{(N_{flap})}\left\{\bar{\Delta}\right\}_m^{*C.T.}$$

$$- \left(r_{11}\right)\left[\bar{C}\right]_m^{(N_{flap})}\left\{\bar{\Delta}\right\}_m^{*fea} = 0 \qquad (72)$$

In summary, Equations (62), (65), (70), and (72) provide (in conjunction with the swash-plate equations of motion previously developed) the essentials necessary to close the system. Equation (57) will provide the basis for obtaining blade mode shapes.

Development of the Final Matrix Equations Governing Dynamic Behavior of Rotor Blades Coupled Through a Swash-Plate

Consider the governing Equation (33) for the swash-plate as developed earlier. In order to make the expression more concise, certain complex functions can be defined. Towards this end Equation (33) is first recast into the following form:

$$\sum_{n=-\infty}^{\infty} \sum_{\ell=-\infty}^{\infty} \left\{ \left[m(s^2 - 2i\ell\Omega s - \ell^2\Omega^2) + \frac{2\pi}{R^3} \frac{\ell^2(\ell^2-1)^2}{\left(\frac{1}{GJ_T} + \frac{\ell^2}{EJ_z}\right)} \right] \delta_q^{\ell}\delta_0^n \right.$$

$$+ \sum_{j=1}^{N_{e.s.}} [k_j + (s - i\ell\Omega)c_j]\delta_0^n\delta_q^{\ell}$$

$$+ \sum_{\substack{j=1 \\ \ell\neq q}}^{N_{e.s.}} [k_j + (s - iq\Omega)c_j]e^{-i\chi_j(q-\ell)}\delta_{q-\ell}^n$$

$$\left. - \frac{\left(\sum_{j=1}^{N_{e.s.}} [k_j+(s-iq\Omega)c_j]e^{-iq\chi_j}\right)\left(\sum_{j=1}^{N_{e.s.}} [k_j+(s-iq\Omega)c_j]e^{i\ell\chi_j}\right)}{K+(s-iq\Omega)C+\sum_{j=1}^{N_{e.s.}} [k_j+(s-iq\Omega)c_j]}\delta_{q-\ell}^n \right\} \bar{w}_{\ell}(s-in\Omega)$$

$$= \sum_{m=1}^{N_b} \frac{(\Delta\bar{T})_m}{a_m} e^{-iq\phi_m} \qquad (73)$$

where δ_j^i is the Kronecker delta function defined such that

$$\delta_j^i = 1 \quad \text{for} \quad i = j$$

and

$$\delta_j^i = 0 \quad \text{for} \quad i \neq j$$

The terms in (73) that are multiplied by a $\delta^n_{q-\ell}$ are those terms which arise from the nonuniformity of the swash-plate supports combined with the swash-plate flexibility.

Consider for example the situation where there are three identical concentrated supports (i.e. $N_{e.s.}=3$) equally spaced at 120° apart. The expression

$$\sum_{j=1}^{N_{e.s.}} k_j e^{ipx_j}$$

is then equal to

$$k\left(1 + e^{ip\frac{2\pi}{3}} + e^{ip\frac{4\pi}{3}}\right)$$

Except for p=0 this quantity will be nonzero only when p is an integer multiple of the number of supports. Since the range of q and ℓ need only be from -1 to +1 for the rigid swash-plate case the largest p could be is ±2. Thus, there are only contributions to Equation (73) from the n=0 terms.

For that case, the final blade equations summarized at the end of the last section in conjunction with Equation (73) provide a closed system to solve for all the unknowns.

If, however, the swash-plate is flexible and/or the supports are unequal or not equally spaced, there will be nonzero coefficients in Equation (73) corresponding to the $\bar{w}_\ell(s-in\Omega)$ unknowns for which n is not equal to zero.

It appears that those coefficients cause the system of equations to have more unknowns than equations. However, this is not really the case since there is an implicit relationship between

$$\bar{w}_\ell(s) \quad \text{and} \quad \bar{w}_\ell(s-in\Omega)$$

The way in which that relationship is used in this analysis is to construct more equations from the basic ones by shifting the Laplace transform variable in integer multiples of $i\Omega$. By truncating to a finite number of equations a solution can be obtained. The shifting of the Laplace transform variable is first demonstrated by replacing the variable s by the quantity $(s-ik\Omega)$

throughout Equation (73) where k is an integer. A single form which represents that equation for any k, including the k equal zero case, can then be written as follows:

$$\sum_{n=-\infty}^{\infty}\left[\sum_{\ell=-\infty}^{\infty}\bar{Z}_n^{\ell}\delta_q^{\ell}\delta_k^{n}+\sum_{\substack{\ell=-\infty\\ \ell\neq q}}^{\infty}\bar{X}_{q,\ell}^{k,n}\,\delta_{k+q}^{n+\ell}\right]=\sum_{m=1}^{N_b}\frac{\Delta\bar{T}_m(s-ik\Omega)}{a_m}\,e^{-iq\phi_m} \tag{74}$$

where:

$$\bar{Z}_n^{\ell}\triangleq m[(s-in\Omega)^2-2i\ell\Omega(s-in\Omega)-\ell^2\Omega^2]$$

$$+\frac{2\pi}{R^3}\,\frac{\ell^2(\ell^2-1)^2}{\left(\frac{\ell^2}{EJ_z}+\frac{1}{GJ_T}\right)}+\sum_{j=1}^{N_{e.s.}}(C_n^{\ell})_j$$

$$-\frac{\left(\sum_{j=1}^{N_{e.s.}}(C_n^{\ell})_j e^{-i\ell\chi_j}\right)\left(\sum_{j=1}^{N_{e.s.}}(C_n^{\ell})_j e^{i\ell\chi_j}\right)}{K+(s-in\Omega-i\ell\Omega)C+\sum_{j=1}^{N_{e.s.}}(C_n^{\ell})_j}$$

$$\bar{X}_{q,\ell}^{k,n}=\sum_{j=1}^{N_{e.s.}}e^{-ix_j(q-\ell)}(C_n^{\ell})_j$$

$$-\frac{\left(\sum_{j=1}^{N_{e.s.}}e^{-iqx_j}(C_n^{\ell})_j\right)\left(\sum_{j=1}^{N_{e.s.}}e^{i\ell\chi_j}(C_n^{\ell})_j\right)}{K+(s-ik\Omega-iq\Omega)C+\sum_{j=1}^{N_{e.s.}}(C_n^{\ell})_j}$$

$$(C_n^{\ell})_j\triangleq k_j+(s-in\Omega-i\ell\Omega)c_j$$

Note that $(\overline{\Delta T})_m$ which appears in Equation (74) is related to the blade input $\left\{\bar{\Delta}\right\}_m^{*C.T.}$ through Equation (68).

Because of the coupling between blades and swash-plate it is necessary to generalize the final blade governing equations as well, through use of the shifting procedure on the Laplace transform variable. For example, the blade control torque Equation (70) is generalized as follows by replacing s by s-ikΩ:

$$
\begin{aligned}
&- a_m^2(1 + (s - ik\Omega)\tau_m)\left(r_3\right)\left[\bar{B}_k\right]_m^{(N_{C.T.})}\left\{\bar{S}_k\right\}_m^{*Tip} \\
&\quad + k_m^{-1}\left(r_4\right)\left[\bar{\lambda}_k\right]_m^{C.T.}\left\{\bar{\Delta}_k\right\}_m^{*C.T.} \\
&+ a_m^2(1 + (s - ik\Omega)\tau_m)\left(r_3\right)\left[\bar{d}_k\right]_m^{(N_{C.T.})}\left\{\bar{\Delta}_k\right\}^{*flap} \\
&\quad + \sum_{\ell=-\infty}^{\infty} a_m(1 + (s - ik\Omega)\tau_m)e^{i\ell\phi_m}\,\bar{w}_\ell(s - ik\Omega) = 0
\end{aligned}
\tag{75}
$$

The k subscript within the vectors and matrices indicates that s has been replaced by (s - ikΩ). Similar generalizations are made of Equations (62), (65), and (72).

The complete set of equations governing the system are written in matrix form as follows:

$$
\sum_{n=-N_f}^{N_f}\left[\bar{T}\right]_n^k\left\{\bar{q}_n\right\}^* = \left\{0\right\} \qquad k = 0, \pm 1, \ldots \pm N_f \tag{76}
$$

where the summation over n has been truncated to range from $-N_f$ to $+N_f$. The quantity $\left\{\bar{q}_n\right\}^*$ contains all of the unknowns, which may include the swash-plate deflections $\bar{w}_\ell$; the blade tip unknowns $\left\{\bar{S}\right\}_m^{*Tip}$ for each blade; and the control torque, $\left\{\bar{\Delta}\right\}^{*C.T.}$,

feathering angle $\left\{\bar{\Delta}\right\}^{*fea}$, and flap angle $\left\{\bar{\Delta}\right\}^{*flap}$ for each blade. The number of spacial harmonics retained in the swash-plate is truncated by letting the summation over ℓ indicated in Equation (74) range from $-N_{max}$ to $+N_{max}$.

A detailed display of the $\left[\bar{T}\right]_n^k$ array and $\left\{\bar{q}_n\right\}^*$ is provided as follows for the case of a three-bladed rotor and a rigid swash-plate (N_{max} equals 1).

$$\left[\bar{T}\right]_n^k = \left[\begin{array}{c|c|c|c} \bar{S}_n^k & \bar{v}_{n1}^k & \bar{v}_{n2}^k & \bar{v}_{n3}^k \\ \hline \bar{C}_1^k \delta_n^k & \bar{B}_1^k \delta_n^k & 0 & 0 \\ \hline \bar{C}_2^k \delta_n^k & 0 & \bar{B}_2^k \delta_n^k & 0 \\ \hline \bar{C}_3^k \delta_n^k & 0 & 0 & \bar{B}_3^k \delta_n^k \end{array}\right] ; \quad \left\{\bar{q}_n\right\}^* = \begin{array}{l} \left\{\bar{r}_n\right\} \text{ swash-plate} \\ \left\{\bar{p}_n\right\}_1 \text{ blade} \\ \left\{\bar{p}_n\right\}_2 \text{ blade} \\ \left\{\bar{p}_n\right\}_3 \text{ blade} \end{array} \tag{77}$$

where:

$$\left[\bar{S}_{nm}^k\right] = \left[\begin{array}{c|c|c} \bar{Z}_n^{-1} \delta_k^n & \bar{X}_{-1,0}^{k,n} \delta_{k-1}^n & \bar{X}_{-1,1}^{k,n} \delta_{k-1}^{n+1} \\ \hline \bar{X}_{0,-1}^{k,n} \delta_k^{n-1} & \bar{Z}_n^0 \delta_k^n & \bar{X}_{0,1}^{k,n} \delta_k^{n+1} \\ \hline \bar{X}_{1,-1}^{k,n} \delta_{k+1}^{n-1} & \bar{X}_{1,0}^{k,n} \delta_{k+1}^n & \bar{Z}_n^1 \delta_k^n \end{array}\right] \tag{78}$$

contains the swash-plate impedances;

$$\left[\bar{\mathcal{D}}^{k}_{nm}\right] = \left(\begin{array}{c|c|c|c} & & \frac{(r_4)}{a_m}\left[\bar{\lambda}_k\right]_m \text{C.T.}\, e^{i\phi_m} & \\ \hline \leftarrow 7 \text{ cols.} \rightarrow \text{ of zeros} & \leftarrow 2 \text{ cols.} \rightarrow \text{ of zeros} & \frac{(r_4)}{a_m}\left[\bar{\lambda}_k\right]_m \text{C.T.} & \leftarrow 2 \text{ cols.} \rightarrow \text{ of zeros} \\ \hline & & \frac{(r_4)}{a_m}\left[\bar{\lambda}_k\right]_m \text{C.T.}\, e^{-i\phi_m} & \end{array}\right) \tag{79}$$

couples the swash-plate to the blade;

$$\left[\bar{B}^{k}_{m}\right] = \left(\begin{array}{c|c|c|c} \left[\alpha\right]\left[\bar{B}_k\right]^{(NS)}_m & -\left[\alpha\right]\left[\bar{C}_k\right]^{(NS)}_m & -\left[\alpha\right]\left[\bar{b}_k\right]^{(NS)}_m & -\left[\alpha\right]\left[\bar{d}_k\right]^{(NS)}_m \\ \hline (r_4)\left[\bar{B}_k\right]^{(N_{fea})}_m & 0 & -(r_4)\left[\bar{b}_k\right]^{(N_{fea})}_m & -(r_4)\left[\bar{d}_k\right]^{(N_{fea})}_m \\ \hline -a_m \bar{Y}^{k}_{m}(r_3)\left[\bar{B}_k\right]^{(N_{C.T.})}_m & 0 & k_m^{-1}(r_4)\left[\bar{\lambda}_k\right]^{(C.T.)}_m & a_m \bar{Y}^{k}_{m}(r_3)\left[\bar{d}_k\right]^{(N_{C.T.})}_m \\ \hline (r_{11})\left[\bar{B}_k\right]^{(N_{flap})}_m & -(r_{11})\left[\bar{C}_k\right]^{(N_{flap})}_m & -(r_{11})\left[\bar{b}_k\right]^{(N_{flap})}_m & 0 \end{array}\right) \tag{80}$$

with $\bar{Y}^{k}_{m} = a_m[1 + \tau_m(s - ik\Omega)]$ (81)

provides the generalized impedances of the $m^{\underline{th}}$ blade;

$$\left[\bar{C}_m^k\right] = \left(\begin{array}{c|c|c} 0 & 0 & 0 \\ \hline 0 & 0 & 0 \\ \hline \bar{Y}_m^k e^{-i\phi_m} & \bar{Y}_m^k & \bar{Y}_m^k e^{i\phi_m} \\ \hline 0 & 0 & 0 \end{array}\right) \tag{82}$$

couples the blades to the swash-plate motion.

Finally,

$$\left\{\bar{r}_n\right\}^{\text{swash-plate}} = \begin{Bmatrix} \bar{w}_{-N_{max}}(s-in\Omega) \\ \cdot \\ \cdot \\ \bar{w}_{-1}(s-in\Omega) \\ \bar{w}_0(s-in\Omega) \\ \bar{w}_1(s-in\Omega) \\ \cdot \\ \cdot \\ \cdot \\ \bar{w}_{N_{max}}(s-in\Omega) \end{Bmatrix} \text{ and } \left\{\bar{p}_n\right\}_m^{\text{blade}} = \begin{Bmatrix} \left\{\bar{S}_n\right\}_m^{*\text{Tip}} \\ \left\{\bar{\Delta}_n\right\}_m^{*\text{fea}} \\ \left\{\bar{\Delta}_n\right\}_m^{*\text{C.T.}} \\ \left\{\bar{\Delta}_n\right\}_m^{*\text{flap}} \end{Bmatrix} \tag{83}$$

The next section discusses the solution scheme starting with Equation (76) as the governing matrix equations for the swash-plate coupled rotor blade system.

Solution Scheme for Obtaining Eigenvalues and Eigenvectors

The solution scheme for obtaining eigenvalues and eigenvectors used in this study is based on an approach referred to in Reference (1) as the Modified Transfer-Matrix Method.

The fundamental purpose of the method is that it avoids the problem of having to compute small differences of large numbers which is commonly known to occur in associated matrix techniques, especially when the frequency determinant is evaluated near the higher natural frequencies. This is accomplished by iterating for the eigenvectors of the system simultaneously with the eigenvalues.

Recall that the starred vector quantities

$$\left\{\bar{S}_n\right\}^{*Tip} \quad , \quad \left\{\bar{\Delta}_n\right\}^{*fea} \quad , \quad \left\{\bar{\Delta}_n\right\}^{*C.T.} \quad , \quad \text{and} \quad \left\{\bar{\Delta}_n\right\}^{*flap}$$

each had unity for its first element as shown in Equations (41), (42), and (55). This is connected with the fact that the actual tip unknowns and discontinuities were considered to be the sum of trial values and correction-type quantities, the latter of which are to be obtained from the solution to Equation (76).

Those values of unity which occur in $\left\{\bar{q}_n\right\}^*$ are removed if the columns in $\left[\bar{T}\right]_n^k$ corresponding to the locations of the unity elements are added together and brought over to the right-hand side of Equation (76) with a minus sign. In addition a set of initial guesses for the swash-plate unknowns are also placed into the analysis so that all quantities solved for will be corrections for the initially assumed values. The final form taken for Equation (76) is then given by

$$\sum_{n=-N_f}^{N_f} \left[A\right]_n^k \left\{\bar{\varepsilon}_n\right\} = \left\{\bar{f}_k\right\} \tag{84}$$

$$k = 0, \pm 1, \pm 2 \ldots \pm N_f$$

where:

$\left[\bar{\bar{A}}\right]^k_n$ is a square array derived from $\left[\bar{\bar{T}}\right]^k_n$ by removing the above mentioned columns.

$\left\{\bar{\varepsilon}_n\right\}$ is the same as $\left\{\bar{q}_n\right\}^*$ except that the unity values are removed.

It can be shown that the quantity $\left\{\bar{f}_k\right\}$ satisfies the following equation.

$$\left\{\bar{f}_k\right\} = - \sum_{n=-N_f}^{N_f} \left[\bar{\bar{A}}\right]^k_n \left\{\bar{\lambda}_k\right\} \tag{85}$$

where: The $\left\{\bar{\lambda}_k\right\}$ are the trial initialization values of the eigenvector. The reason that $\left\{\bar{f}_k\right\}$ is not directly computed in this way is related to the numerical problems that the modified transfer matrix technique is designed to avoid.

The manner in which Equation (84) is used to obtain the eigenvalues and eigenvectors can be best shown by a simple example. Consider a system for which the final homogeneous matrix equation consists of only three equations as follows:

$$\begin{pmatrix} a_{11} & a_{12} & a_{13} \\ a_{21} & a_{22} & a_{23} \\ a_{31} & a_{32} & a_{33} \end{pmatrix} \begin{Bmatrix} X_1 \\ X_2 \\ X_3 \end{Bmatrix} = \begin{Bmatrix} 0 \\ 0 \\ 0 \end{Bmatrix} \tag{86}$$

where the a_{ij} are polynomial functions of a trial eigenvalue s.

If the trial eigenvalue is an actual eigenvalue of the system, then it is well-known that the determinant of the 3 x 3 a_{ij} matrix must vanish. Thus,

$$\left|a_{ij}\right|_{s=s_n} = 0$$

In the more standard transfer matrix procedure, this fact is used directly to find the eigenvalue through a minimization of the determinant. It usually happens, however, that for higher natural frequencies the determinant gets hit by round-off error very soon since the determinant calculation involves taking small differences of large numbers.

The modified approach would proceed as follows:

Let

$$\begin{Bmatrix} X_1 \\ X_2 \\ X_3 \end{Bmatrix} = \begin{bmatrix} \lambda_1 & 1 & 0 & 0 \\ \lambda_2 & 0 & 1 & 0 \\ \lambda_3 & 0 & 0 & 1 \end{bmatrix} \begin{Bmatrix} 1 \\ \varepsilon_1 \\ \varepsilon_2 \\ \varepsilon_3 \end{Bmatrix} \tag{87}$$

and substitute into Equation (86), This results in

$$\begin{bmatrix} (\lambda_1 a_{11} + \lambda_2 a_{12} + \lambda_3 a_{13}) & a_{11} & a_{12} & a_{13} \\ (\lambda_1 a_{21} + \lambda_2 a_{22} + \lambda_3 a_{23}) & a_{21} & a_{22} & a_{23} \\ (\lambda_1 a_{31} + \lambda_2 a_{32} + \lambda_3 a_{33}) & a_{31} & a_{32} & a_{33} \end{bmatrix} \begin{Bmatrix} 1 \\ \varepsilon_1 \\ \varepsilon_2 \\ \varepsilon_3 \end{Bmatrix} = \begin{Bmatrix} 0 \\ 0 \\ 0 \end{Bmatrix} \tag{88}$$

Removing the first column of the matrix and bringing it to the right-hand side with a minus sign yields

$$\begin{bmatrix} a_{11} & a_{12} & a_{13} \\ a_{21} & a_{22} & a_{23} \\ a_{31} & a_{32} & a_{33} \end{bmatrix} \begin{Bmatrix} \varepsilon_1 \\ \varepsilon_2 \\ \varepsilon_3 \end{Bmatrix} = - \begin{Bmatrix} f_1 \\ f_2 \\ f_3 \end{Bmatrix} \tag{89}$$

where

$$f_i = \sum_{j=1}^{3} \lambda_j a_{ij} \qquad i = 1, 2, 3 \tag{90}$$

If the quantity X_1 is normalized to unity and λ_1 is set equal to unity then ε_1 is clearly zero. Therefore

$$\begin{bmatrix} a_{12} & a_{13} \\ a_{22} & a_{23} \\ a_{32} & a_{33} \end{bmatrix} \begin{Bmatrix} \varepsilon_2 \\ \varepsilon_3 \end{Bmatrix} = \begin{Bmatrix} f_1 \\ f_2 \\ f_3 \end{Bmatrix} \tag{91}$$

With three equations and two unknowns a solution can be obtained for ε_2 and ε_3 by taking any two of the three equations. For example, the equation

$$\begin{bmatrix} a_{12} & a_{13} \\ a_{22} & a_{23} \end{bmatrix} \begin{Bmatrix} \varepsilon_2 \\ \varepsilon_3 \end{Bmatrix} = \begin{Bmatrix} f_2 \\ f_3 \end{Bmatrix} \tag{92}$$

can easily be solved for those unknowns.

Give the solutions to (92) the names $\varepsilon_2^{(1)}$ and $\varepsilon_3^{(1)}$. If these values were substituted into the third equation, that equation would be identically satisfied only if the trial eigenvalue s had been an actual eigenvalue s_n, since only then are the three equations dependent.

Furthermore, if only $\varepsilon_2^{(1)}$ is substituted into the third equation another value for ε_3 may be obtained. That is,

$$\varepsilon_3^{(2)} = (f_3 - a_{32}\, \varepsilon_2^{(1)}) a_{33} \tag{93}$$

The difference between $\varepsilon_3^{(2)}$ and $\varepsilon_3^{(1)}$ is a measure of how close the trial eigenvalue is to the actual eigenvalue.

Thus the process of minimizing this difference which is referred to as a remainder will establish the eigenvalue. It is essentially a generalization of this procedure which comprises the modified transfer matrix technique.

Returning to Equation (84), the procedure taken in the general case is to first remove a column of the coefficient array corresponding to the reference unknown in the normalization process. A row is then removed from the coefficient array, and the condensed array is solved for the epsilons with all but one then inserted into the removed row in order to obtain a second value for the non-substituted epsilon. As in the simple example described previously, a remainder quantity is then computed.

After the epsilons and the remainders have been computed the epsilons are added to the lambda-type quantities as follows

$$\left\{\bar{\lambda}_k\right\}^{(new)} = \left\{\bar{\lambda}_k\right\}^{(old)} + \left\{\bar{\varepsilon}_k\right\} \tag{94}$$

A new trial value of the eigenvalue is assumed in all of the blade transfer matrices and swash-plate impedances and the coefficient matrix is rederived. This requires transferring along the blades again with the new starting values for the $\bar{\lambda}$-type quantities as required in Equations (41) and (56).

This process is repeated until the eigenvalue has converged to within a predetermined number of significant figures. The order of magnitude of the remainder is typically seen to drop during the process to a very small number compared to the values computed during the first one or two passes..for example from 10^{5} to 10^{-12}.

After a converged result has been obtained, a final pass is made along the blades with the last eigenvalue used to compute and print out the blade mode shapes. This is done through use of Equation (57).

For each station along the $m^{\underline{th}}$ blade the arrays

$$\left[\bar{B}\right]_m^{(i)}, \quad \left[\bar{b}\right]_m^{(i)}, \quad \left[\bar{C}\right]_m^{(i)}, \text{ and } \left[\bar{d}\right]_m^{(i)}$$

are constructed and the products with the starred quantities, which contain the last set of $\left\{\bar{\varepsilon}\right\}$'s computed, are carried out. This gives numerical values for the $\left\{\bar{S}\right\}_m^{(i)}$ for every station of each blade.

DESCRIPTION OF COMPUTER PROGRAM

The computer program developed in this study is an overlay structured program composed of one root segment, three primary segments, and four secondary segments (see Figure 5). The root, or main, segment is the controlling section of the total program, calling subsequent portions of the program into central core as needed.

The program uses card input data and has required 65015_8 locations on a CDC 6600 computer during checkout. The storage required may vary slightly from system to system because of different software. The compiler used was the standard RUN compiler (FTNDEV in Toronto), and the SCOPE system manual was referenced for all program problems. To facilitate debugging, separate overlay files were created and written on disk for the root segment, and each of the primary segments. This also enabled bypassing of the LOAD and NOGO steps during testing stages.

To execute, the main segment is loaded into central memory by the system LOADER and control is passed to the first executable statement. The main segment calls for the secondary overlay segment which reads input data into core first. This segment subroutine, SETUP, creates a storage vector containing data for all stations. Control is returned to the main segment which calls a matrix-creating secondary segment into core, thus overlaying the SETUP segment. From this control is again returned to main which calls one of the two remaining primary overlay segments into core for execution, overlaying the first primary segments. Control then returns to the main line.

The primary segment, MID(2,0), is a non-executing program whose only purpose is to store several large labelled common areas, which would otherwise use valuable storage space in the permanently resident main segment. In addition, to reduce the necessary amount of core storage, one of the larger arrays used by the subroutines in this segment is stored temporarily on tape when the second or third primary segment is in core.

The second and third primary segments are executing segments, with the primary level QSOLN being called in the forced vibration case, and the primary level EPSOLN being called in the free vibration case. During execution, these segments would overlay the primary segment MID(2,0), perform their solution obtaining service, and return control to the main segment upon completion. The main segment may then restart the cycle or end program execution upon satisfaction of data requirements.

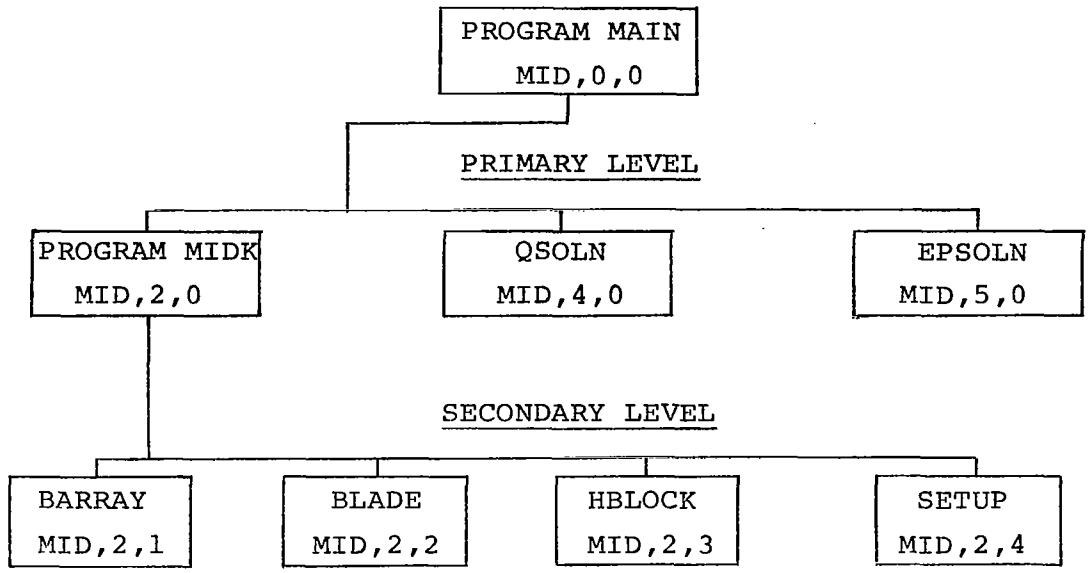

Subroutines Contained in Above Segments

MID,0,0
MAIN LINE

MID,2,0
MIDK

MID,2,1
BARRAY
RIGID
BEND
STIFF
MLRC1
MLRC2
MLCC2
ELAST
MLCC1
MULTC
CMAT
MASSB

MID,2,2
BLADE
YKM

MID,2,3
HBLOCK

MID,2,4
SETUP
PHASE
SUPPHA
YA
BYE
YSK
BYB
YRIGID

MID,4,0
QSOLN
FKNS
MULTC
CMAT

MID,4,1
TKNS
YKM
ZLN
EXPON
EXCHI
XNLQ

MID,5,0
EPSOLN
YKM
MULTC
CMAT
EXCOL
EXROW
EXRFFT
INRIFT

MID,5,1
TKNS
ZLN
EXPON
EXCHI
XNLQ

MID,5,2
FTFTKN

MID,5,4
AFTKN

Overlay structure of computer program

Description of Input Data

Consistent units of length, time, force must be used on all input data. All angles are input in radians.

Unless otherwise stated the following input cards are read from Subroutine SETUP.

Card #1 Format 10I5

NB — Number of blades. If symmetry of blade motions is assumed, NB=1, and NBS (see Card #3) is equal to the number of blades

NSP — If swash-plate is included in computation, NSP=1. If swash-plate is not included, NSP=0

MAXN — Number of harmonics used to represent swash-plate; if swash-plate is assumed rigid MAXN=1

NES — Number of elastic supports on the swash-plate

IFV — For a forced vibration problem IFV=0; for a free vibration problem IFV=1

NF — Maximum harmonic number to be computed

NSIZEY — Size of dummy Y vector, constant equal to 125

NOUT — File number for writing output, normally NOUT=6

Card #2 Format 10I5

MXIT — Maximum number of iterations to be performed on the solution vector for each eigenvalue

NEXP — Number of significant figures required for convergence of a solution vector

NCONV — Number of the element in the solution vector upon which convergence of the solution vector is based

Card #3

MFLAP — If no flap hinge is included, MFLAP=0. If a flap hinge is to be included, MFLAP=1.

NFEA — Section number at which the feathering axis exists.

NCT — Section number of the blade just after which the control torque is applied through the rocker arm.

NFLAP — Counting from the tip in, NFLAP is the section number just after which the flap hinge exists. If MFLAP=0 make NFLAP>NS.

NS — Number of sections on the blade.

NBS — If symmetry of blade motions is assumed, NBS is set equal to number of blades, otherwise NBS=0.

NPS — Integer describing type of blade symmetry.

NIG — If swash-plate has a spring-damper unit on the support foundation, NIG=1. All other cases NIG=0.

Card #4 is read only if IFV=0 (forced vibration computation).

Card #4 Format 10I5

MINPN — Minimum pole number.

MAXPN — Maximum pole number.

Cards #5 through #7 are read only if IFV=1 (free vibration computation.)

Card #5 Format 10I5

NEGNS — Number of eigenvalues to be found.

MXITER — Maximum number of iterations to be performed on each eigenvalue.

MXEROR — Number of significant figures required for convergence to each eigenvalue.

ITEREM — Number of the element in the remainder vector upon which the iteration scheme is based when ITDET=0.

NORM — Column deleted for normalization purposes from the coefficient matrix.

NREMS — Number of remainders to be computed.

NPRCNT — Increments first eigenvalue guess used to compute second guess, normally NPRCNT=10.

ITDET — If iteration is to proceed on remainders ITDET=0. If iteration is to proceed on determinant values, ITDET=1.

Card #6 Format 16I5

IREM(I), I=1,NREMS
Equation numbers for which remainders are to be computed.

Card #7

EGNS(I), I=1,NEGNS
Values of initial guesses for eigenvalues.

Card #8

CY4 Operating speed, Ω

CY11 Gravity constant g

CY15 Rotor tilt angle, ψ

Cards #9 through #13 are read only if NSP=1.

Card #9

CY13 Torsional rigidity GJ_T for swash-plate.

CY14 Flexural rigidity EJ_Z for swash-plate.

CY20 Mass of swash-plate.

CY39 Radius of swash-plate.

Card #10 is read from Subroutine SUPPHA

Card #10

CHI(J), J=1,NES
Azimuthal locations of swash-plate supports (radians).

Card #11

AK(J), J=1, NES
Stiffnesses of swash-plate supports.

Card #12

AC(J), J=1,NES
Damping values of swash-plate supports.

Card #13

CAPK Stiffness of swash-plate foundation support.

CAPC Damping coefficient of swash-plate foundation support.

Card #14 is read from Subroutine PHASE

Card #14

PHIM(MS), MS=1,NB
Starting azimuth positions of each blade.

Card #15

AKCI(MS), MS=1,NB
Flexibility (inverse stiffness) of push-pull rod spring-damper units.

Card #16

TAU(MS), MS=1,NB
Decay times associated with push-pull rod spring-damper units (seconds).

Card #17

SMLA(MS), MS=1,NB
Rocker arm lengths.

The following cards represent the most general set of data for a section of blade. A set of data must be provided for each section of each blade.

Section parameter control card

Parameter	Associated Matrix	
M1	Mass	Associated matrix is not computed if parameter=0. Associated matrix is computed for a blade section if parameter=1.
M2	Bend	
M3	M3 is always zero	
M4	Elastic	
M5	Rigid	
M6	Stiffness	

Mass data cards (2); do not include if M1=0

Y(1)	mass of segment
Y(2)	local offset of center of mass ahead of neutral axis
Y(3)	radial distance of inboard end of station from axis of rotation
Y(4)	distance of neutral axis ahead of line through axis of rotation
Y(5)	moment of inertia of segment about neutral axis
Y(6)	moment of inertia of segment about chord, normally provided as zero since mass is considered to be concentrated along a chord line
Y(7)	moment of inertia of segment about local normal to blade
Y(8)	local sweep angle Φ as defined in Figure 3
Y(9)	local coning angle Θ as defined in Figure 3
Y(10)	local pitch angle Ψ as defined in Figure 3

Bend data card; do not include if M2=0

Y(8)	=	Φ
Y(9)	=	Θ
Y(10)	=	Ψ

Elastic data card; do not include if M4=0

Y(75)	length of elastic section
Y(76)	torsional stiffness (GJ_T) of blade section
Y(77)	edgewise bending stiffness of section
Y(78)	flapwise bending stiffness of section

Rigid offset data card; do not include if M5=0

Y(99)	offset in x-direction
Y(100)	offset in y-direction
Y(101)	offset in z-direction
Y(102)	local steady axial force
Y(103)	local steady edgewise shear force
Y(104)	local steady flapwise shear force

Concentrated spring data card, do not include if M6=0

Y(105)	flexibility of torsion spring between sections
Y(106)	flexibility of flapwise moment spring between sections
Y(107)	flexibility of edgewise moment spring between sections
Y(108)	torsion spring-damper time constant
Y(109)	flapwise spring-damper time constant
Y(110)	edgewise spring-damper time constant

APPLICATION OF PROGRAM

The program developed in this study was used to analyze representative models of the OH-6A four-bladed rotor system and the three-bladed XH-51 rotor system. Calculations of the effect of swash-plate support asymmetry were restricted to the OH-6A because the XH-51 pitch control is passed through a relatively massive gyro stabilizer which minimizes the effect of the swash-plate and its support flexibilities. Calculations of the effect of blade mismatch were made for both systems. The results obtained are presented and discussed below.

Studies of the OH-6A Rotor System

The blade data (Table I) used for the OH-6A was obtained from information developed by the manufacturer. Values for the lateral, longitudinal, and collective control system stiffness, in addition

to a control stiffness which is recommended for standard single blade vibration analyses, were also obtained from manufacturer data. Data for the mass and flexibility of the swash-plate itself was not available. Thus, values were used which seemed reasonable based on the dimensions of the OH-6A rotor system.

TABLE I

BASIC CHARACTERISTICS OF OH-6A MODEL

Blade length	4.0005 meters
Blade torsional inertia	0.05455 kilograms-meters^2
Blade mass	17.9663 kilograms
Swash-plate mass	6.9469 kilograms
Control system stiffnesses:	
lateral	2001.53 Newton-meters/radian
longitudinal	735.03 Newton-meters/radian
collective	185.45 Newton-meters/radian

The initial calculations carried out with this program for the OH-6A were to predict blade frequencies and mode shapes using the single blade option of the program. This option ignores the flexibility and mass of the swash-plate and uses a representative control system stiffness which accounts for the flexibility of the push-pull rods, and the swash-plate support flexibilities. Using the single blade option with the representative control system stiffness specified by the manufacturer, the results shown in Table II were obtained.

TABLE II

SINGLE BLADE MODES AND FREQUENCIES FOR THE OH-6A

Mode Identifier	σ(sec^{-1})	ω(rad/sec)
1st torsion	-1.27×10^{-2}	152.48
2nd torsion	-3.55×10^{-2}	354.84
1st flap	-3.3×10^{-4}	51.47
2nd flap	-.85	124.14
3rd flap	-.82	213.44
4th flap	-9.43	395.02
5th flap	-1.38	522.76
6th flap	-11.64	740.68
1st edgewise	-2.32	23.10
2nd edgewise	-16.39	230.68
3rd edgewise	-28.05	627.63

The above are eigenvalues for a single blade but with full coupling between torsion, flap, and edgewise degrees-of-freedom (including gyroscopic effects). The rotor system operating speed is 50.065 rad/sec. The negative σ's indicate a stable damping rate for each of these vibration modes.

Uniform Supports.-In investigating the mass-elastic effects of the swash-plate on rotor stability and vibration frequencies, the blade torsional and feathering modes are most likely to be affected since the hub is held fixed in this analysis and the blades are only coupled together through the pitch control mechanism. The initial set of computer runs for the swash-plate coupled OH-6A system was directed at finding the modes and eigenvalues of interest for the case of uniform supports. The swash-plate was assumed to be rigid and supported by three equal springs spaced 120° apart. The lateral and longitudinal cyclic stiffnesses for this symmetric case were set equal to the mean of their actual values which are shown in Table I. The complex eigenvalues found for this nominal set of conditions are listed in Table III with their modal identification.

Figures 5, 6, and 7 present a visual picture of the rotor blade and swash-plate response corresponding to representative cyclic and collective modes listed in Table III. For example, in the table the first two torsion modes at 125.7 (2T) and 149.1 (3T) represent cyclic modes, whereas the torsion mode at 288.0 (5T) indicates a collective mode. The intermediate mode at 215.9 (4T) is a reactionless mode in which the resultant forces and moments acting on the swash-plate from the blades all cancel so that the swash-plate remains motionless. A comparison with Table II (single blade frequencies) indicates that coupling of the blades through the swash-plate introduces additional torsion modes which were not predicted with the single blade analysis. On the other hand, the flap and edgewise modes found in the coupled case were very close to values found in the single blade analysis.

The blade tip torsional displacements for each blade are also shown in Table III. It can be shown that the following meaning can be attached to each number set appearing under the Blade Tip Deflection columns in Table III.

(1, 1, 1, 1) $\sim$	umbrella mode	(5T), (7T)
(1, -i, - 1, i) $\sim$	forward whirl mode	(2T), (6T), (1E), (2F)
(1, i, - 1, -i) $\sim$	backward whirl mode	(3T), (1F)
(1, -1, 1, -1) $\sim$	reactionless mode	(4T)

It should be noted from the sign of the real part of the eigenvalues that all of the modes for this case are stable except for the reactionless mode (4T) which is unstable. The

TABLE III

OH-6A NOMINAL CASE - UNIFORM SUPPORTS

	Eigenvalue		Blade Tip Deflections				Blade Root Deflections				Swash-Plate Response in Each Harmonic		
	σ	ω	1	2	3	4	1	2	3	4	$\bar{w}_{-1}$	$\bar{w}_0$	$\bar{w}_1$
T	-.05	125.7	+1.0	-1.0i	-1.0	+1.0i	+.79	-.79i	-.79	+.79i	+.30	0	0
T	-.011	149.1	+1.0	+1.0i	-1.0	-1.0i	+.70	+.70i	-.70	-.70i	0	0	+.22
T	+.096	215.9	+1.0	-1.0	+1.0	-1.0	+.38	-.38	+.38	-.38	0	0	0
T	-.0013	288.0	+1.0	+1.0	+1.0	+1.0	-.01	-.01	-.01	-.01	0	-.149	0
T	-.003	298.3	+1.0	-1.0i	-1.0	+1.0i	-.06	+.06i	+.06	-.06i	-.155	0	0
T	-.04	450.0	+1.0	+1.0	+1.0	+1.0	-.72	-.72	-.72	-.72	0	+.27	0
E	-16.3	230.6	+1.0	-1.0i	-1.0	+1.0i	0	0	0	0	+.0045 +.0072i	0	0
F	-.02	51.63	+1.0	+1.0i	-1.0	-1.0i	+.94	+.94i	-.94	-94i	0	0	+.024
F	-.87	213.2	+1.0	-1.0i	-1.0	+1.0i	+.56 +.015i	-.56i +.015	-.56 -.015i	+.56i -.015	-.016 -.003i	0	+.0045i 0

T - Torsion Mode - deflection is normalized torsion angle

E - Edgewise Mode - deflection is normalized edgewise deflection

F - Flapwise Mode - deflection is normalized flapwise slope

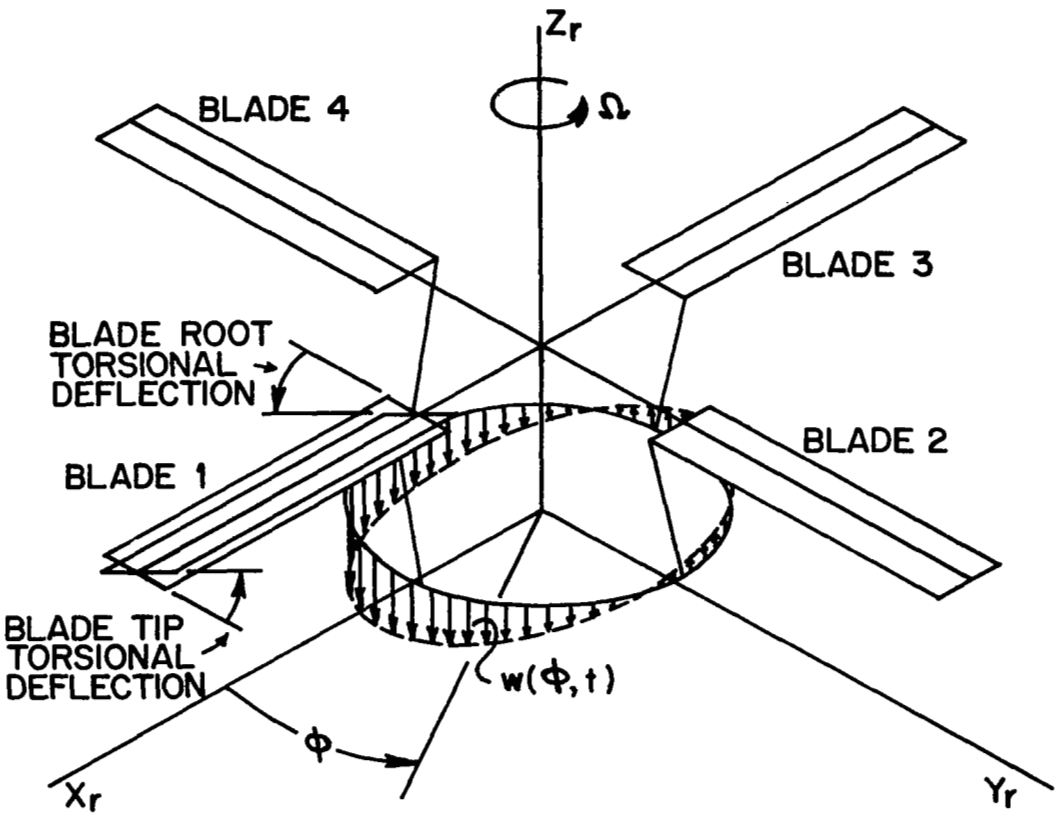

Figure 5. Generalized real time motion of rotor blades and swash-plate - (see Table III)

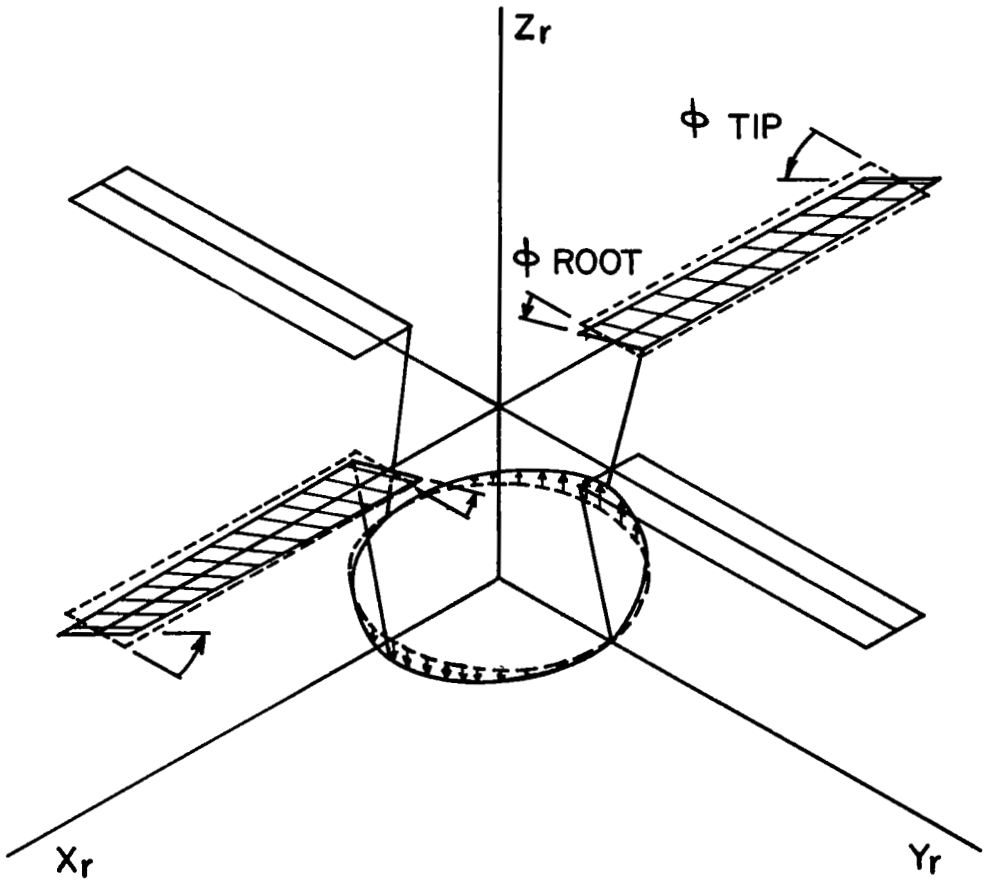

Figure 6. In-phase cyclic mode of OH-6A (see Table III, 2T and 3T)

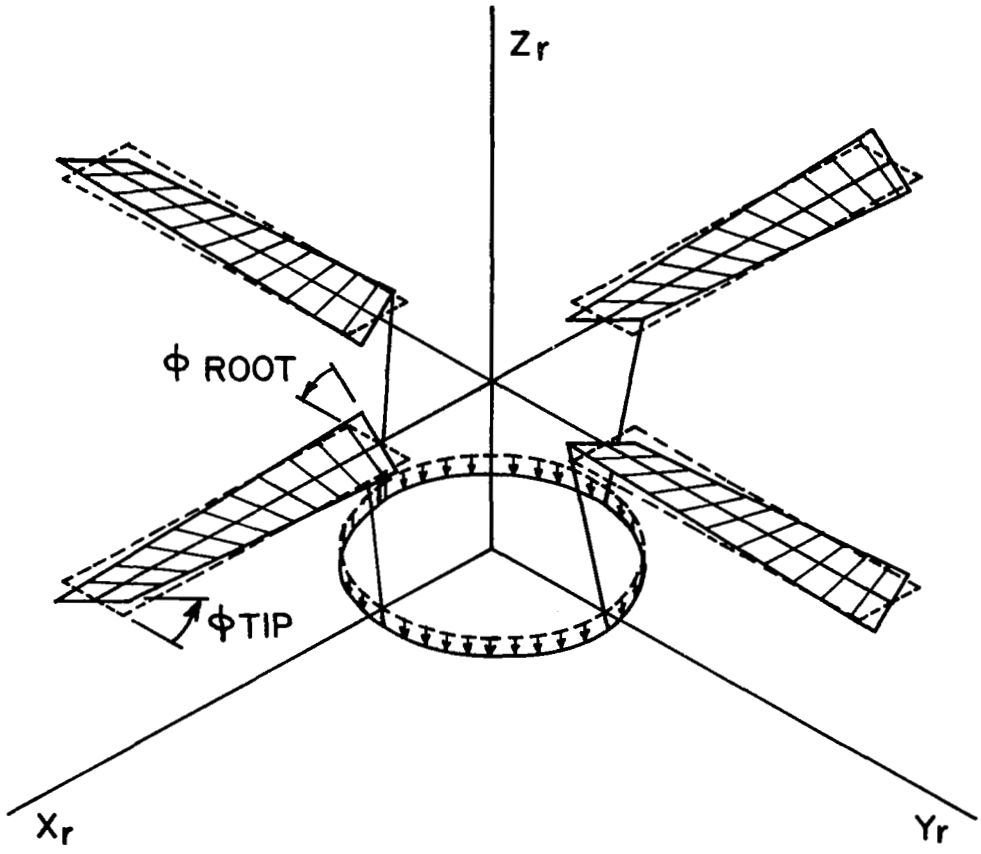

Figure 7. Out-of-phase umbrella mode of OH-6A (see Table III, 5T)

reasons for this instability are not conclusive, but it is believed to be associated with feathering-edgewise coupling and the presence of a damper across the lead-lag hinge. More study is required of this phenomenon.

Simple Model.-In order to gain an insight as to how swash-plate coupling affects the vibratory modes of a rotor system, a simple model was used to represent the ehavior of the OH-6A system while vibrating in its rigid body feathering modes. Very simply, the model consisted of rigid, completely uniform, untwisted rotor blades, devoid of any offsets which could couple degrees-of-freedom. Values of the blade torsional inertia, mass, and control system properties were the same as in the nominal OH-6A case described previously.

This simplified case was run on the computer to obtain all eigenvalues. In addition closed form solutions were developed so that the basis of each mode could be better understood. Numerical results for the simplified case are presented in Table IV. Note that the eigenvalue at ω = 129.2 rad/sec is clearly the counterpart of the mode having a frequency of 125.7 rad/sec that was listed for the OH-6A in Table III (Nominal case of flexible blades on uniformly supported swash-plate).

Closed Form Solutions:-The closed form solutions obtained for the simple case indicate that if the swash-plate mass is neglected, the frequencies of 129.2 and 156.3 would coalesce to a single frequency of 166.475 rad/sec. Similarly, the frequency of the collective mode would change from 59.2 to 76.9 rad/sec. The higher frequency modes of 387.9, 395.0 and 468.0 rad/sec are predominantly modes that arise from the mass coupling of the swash-plate with the blades and are not predicted if either the swash-plate mass or blade inertia is made zero. This is substantiated by the fact that as the blade inertia approaches zero the root at 156.3 approaches 288.5, the root at 129.2 approaches 188.4, the root at 59.2 approaches 69.7, and all of the others disappear. The closed form solution also indicates that the reactionless mode which occurs at 254.9 rad/sec in the rigid blade case and 215.9 rad/sec in the nominal OH-6A case is independent of swash-plate mass or swash-plate support stiffness as would be expected.

From a comparison of Tables II (rigid blade model) and III (flexible blade model) it is apparent that for the nominal case, the frequencies of 125.7 and 149.1 rad/sec are the two that arise from swash-plate coupling with the uncoupled blade frequency at 152.9 rad/sec. The frequencies of 288.0 and 298.3 are predominantly associated with swash-plate coupling with rigid body blade feathering. The additional mode at 450.0 rad/sec is not predicted in the simple model since it is a predominantly blade torsion mode and also since the simplified model had rigid blades.

A physical interpretation of the complex numbers occurring in Tables III and IV may be gained by showing the correspondence of

TABLE IV

SIMPLIFIED RIGID BLADE MODEL OF OH-6A - UNIFORM SWASH-PLATE SUPPORTS

	Eigenvalue		Blade Tip Deflections				Blade Root Deflections				Swash-Plate Response in Each Harmonic		
	σ	ω	1	2	3	4	1	2	3	4	$\bar{w}_{-1}$	$\bar{w}_0$	$\bar{w}_1$
1T	0	59.2	+1.0	+1.0	+1.0	+1.0	+1.0	+1.0	+1.0	+1.0	0	0	0
2T	0	129.2	+1.0	-1.0i	-1.0	+1.0i	+1.0	-1.0i	-1.0	+1.0i	+.38	0	0
3T	0	156.3	+1.0	+1.0i	-1.0	-1.0i	+1.0	+1.0i	-1.0	-1.0i	0	0	+ .32
4T	0	254.9	+1.0	-1.0	+1.0	-1.0	+1.0	-1.0	+1.0	-1.0	0	0	0
5T	0	387.9	+1.0	+1.0	+1.0	+1.0	+1.0	+1.0	+1.0	+1.0	0	-.68	0
6T	0	395.0	+1.0	-1.0i	-1.0	+1.0i	+1.0	-1.0i	-1.0	+1.0i	-.38	0	0
7T	0	468.4	+1.0	+1.0i	-1.0	-1.0i	+1.0	+1.0i	-1.0	-1.0i	0	0	-1.23

the Laplace transformed and the more standard real time solutions. It can be shown that for a given vibration mode at $s = \sigma_n + i\omega_n$ the real time solution is related to the complex Laplace transformed solution in the following simple way:

Real time variable

$$X(t) = e^{\sigma_n t} \cos(\omega_m t + \beta)$$

Corresponding transformed variable

$$\bar{X}(S_n) = \bar{X}^{real} + i\,\bar{X}^{imag}$$

$$= \rho\, e^{i\beta}$$

where ρ and β are the modulus and phase angle of the complex number $\bar{X}(S_n)$. Thus if the blade tip unknowns turn out so that the complex torsional displacements $(\bar{\phi}_x)_m(s)$ of each blade of a four-bladed rotor are given by 1, $-i$, -1, and i respectively, then in real time this means:

$$(\phi_x)_1(t) = e^{\sigma t} \cos \omega t$$

$$(\phi_x)_2(t) = e^{\sigma t} \cos(\omega t - \tfrac{\pi}{2})$$

$$(\phi_x)_3(t) = e^{\sigma t} \cos(\omega t - \pi)$$

$$(\phi_x)_4(t) = e^{\sigma t} \cos(\omega t - \tfrac{3\pi}{2})$$

which can be identified as a forward whirl motion since apart from the exponential growth factor a given blade responds at time t as the blade behind it did at a time equal to $t - \frac{\pi}{2\omega}$. Similarly, the real time motion of the swash-plate can be obtained as follows from the $\bar{w}_\ell$'s listed in Tables III and IV.

$$w(\phi,t) = e^{\sigma t} \sum_{\ell=-N_{max}}^{N_{max}} \rho_\ell \cos(\omega t + \beta_\ell + \ell\phi)$$

where in polar form

$$\bar{w}_\ell(s) = \bar{w}_\ell^{real} + i\,\bar{w}_\ell^{imag}$$
$$= \rho_\ell\, e^{i\beta_\ell}$$

Thus, $\bar{w}_\ell$ for positive ℓ corresponds to an apparent backward whirl of the swash-plate at a frequency of ω/ℓ rad/sec described in the rotating frame. For negative ℓ's the w_ℓ gives a contribution to forward whirl. Since the deflection of the swash-plate described in the fixed frame is given by

$$v(\theta,t) = w(\theta - \Omega t, t)$$

$$= e^{\sigma t} \sum_\ell \rho_\ell \cos[(\omega - \ell\Omega)t + \ell\theta + \beta_\ell]$$

it becomes clear that the negative ℓ also always corresponds to forward whirl as viewed from the fixed frame. However, the positive ℓ terms correspond to backward whirl as viewed from the fixed frame only if the frequency part of the eigenvalue is greater than $\ell\Omega$.[1]

Consider for example, the results of the simplified rigid body version of the OH-6A listed in Table IV. The real time blade feathering response and swash-plate motion corresponding to each of the eigenvalues are written in equation form in Table V.

The first equation is for the in-phase umbrella mode which is also shown in Figure 8. Both the 2nd and 3rd modes described in Tables IV and V are cyclic modes in which the swash-plate motion is in phase with the blade root feathering motion. Figure 9 corresponds to either of these in-phase cyclic modes for the time, t=0. Figure 10 corresponds to the reactionless mode at 254 rad/sec, also when t=0.

Asymmetry of Supports:-Using as a basis the results for the nominal OH-6A case listed in Table III (uniform supports), the effect of different lateral and longitudinal control system stiffnesses was investigated. The eigenvalues and mode shapes were calculated with the actual lateral and longitudinal stiffnesses listed in Table I as well as for some less extreme conditions of asymmetry. For the fully asymmetric case corresponding to the actual OH-6A data the significant eigenvalues and corresponding modal quantities are shown in Table VI.

---

[1] Where forward whirl is defined of the form $\cos(\Omega + \omega)t$ and reverse whirl of the form $\cos(\Omega - \omega)t$ with $\omega > \Omega$.

TABLE V

REAL TIME MOTION CORRESPONDING TO EACH MODE FOUND IN RIGID BLADE VERSION OF THE OH-6A

Eigenvalue	Blade Torsional Response	Swash-Plate Response
$i\omega_1$, $\omega_1 = 59.2$	$\Phi_m(t) = \cos \omega_1 t$	$v(\theta,t) = 0.5 \cos \omega_1 t$
$i\omega_2$, $\omega_2 = 129.2$	$\Phi_m(t) = \cos(\omega_2 t - \phi_m)$	$v(\theta,t) = 0.38 \cos[\theta - (\Omega + \omega_2)t]$
		$w(\phi,t) = 0.38 \cos[\phi - \omega_2 t]$
$i\omega_3$, $\omega_3 = 156.3$	$\Phi_m(t) = \cos(\omega_3 t + \phi_m)$	$v(\theta,t) = 0.32 \cos[\theta + (\omega_3 - \Omega)t]$
		$w(\phi,t) = 0.32 \cos[\phi + \omega_3 t]$
$i\omega_4$, $\omega_4 = 254.9$	$\Phi_m(t) = \cos(\omega_4 t - 2\phi_m)$	$v(\theta,t) = w(\phi,t) = 0$
$i\omega_5$, $\omega_5 = 387.9$	$\Phi_m(t) = \cos \omega_5 t$	$v(\theta,t) = w(\theta,t) = - 0.68 \cos \omega t$
$i\omega_6$, $\omega_6 = 395.0$	$\Phi_m(t) = \cos(\omega_6 t - \phi_m)$	$v(\theta,t) = 0.38 \cos[(\omega_6 + \Omega)t - \theta + \pi]$
		$w(\phi,t) = 0.38 \cos[\omega_6 t - \phi + \pi]$
$i\omega_7$, $\omega_7 = 468.4$	$\Phi_m(t) = \cos(\omega_7 t + \phi_m)$	$v(\theta,t) = 1.23 \cos[(\omega_7 - \Omega)t + \theta + \pi]$
		$w(\phi,t) = 1.23 \cos[\omega_7 t + \phi + \pi]$

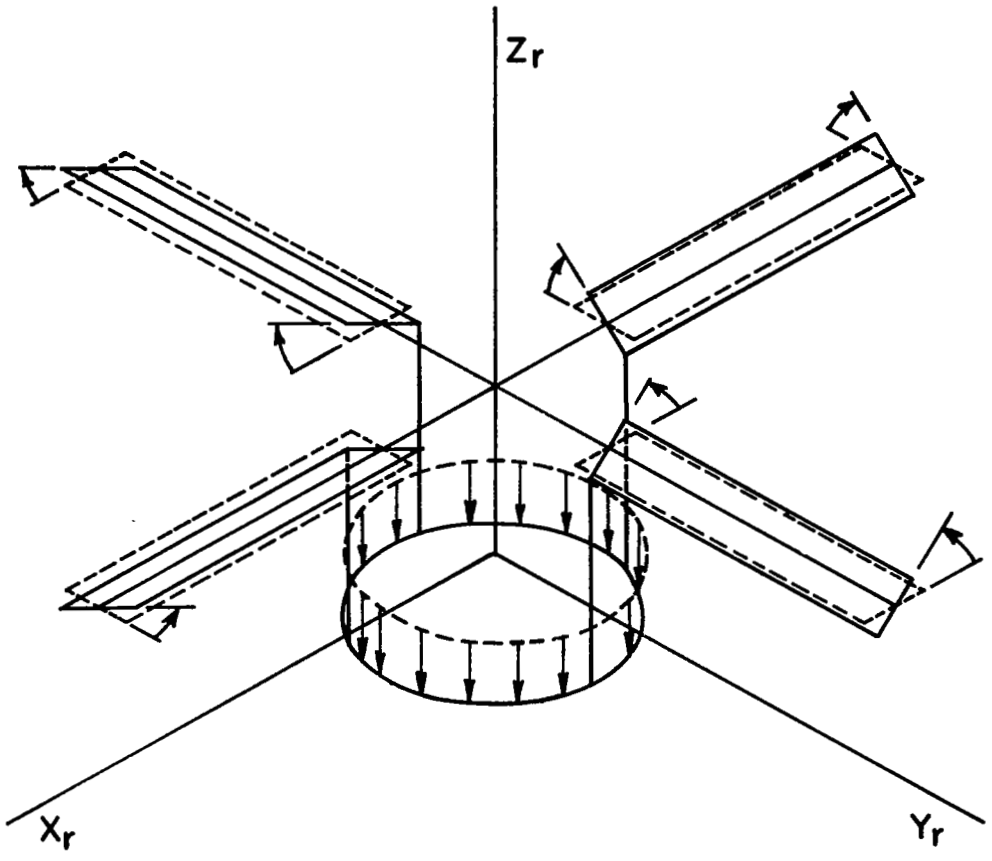

Figure 8. In-phase umbrella mode for simplified OH-6A

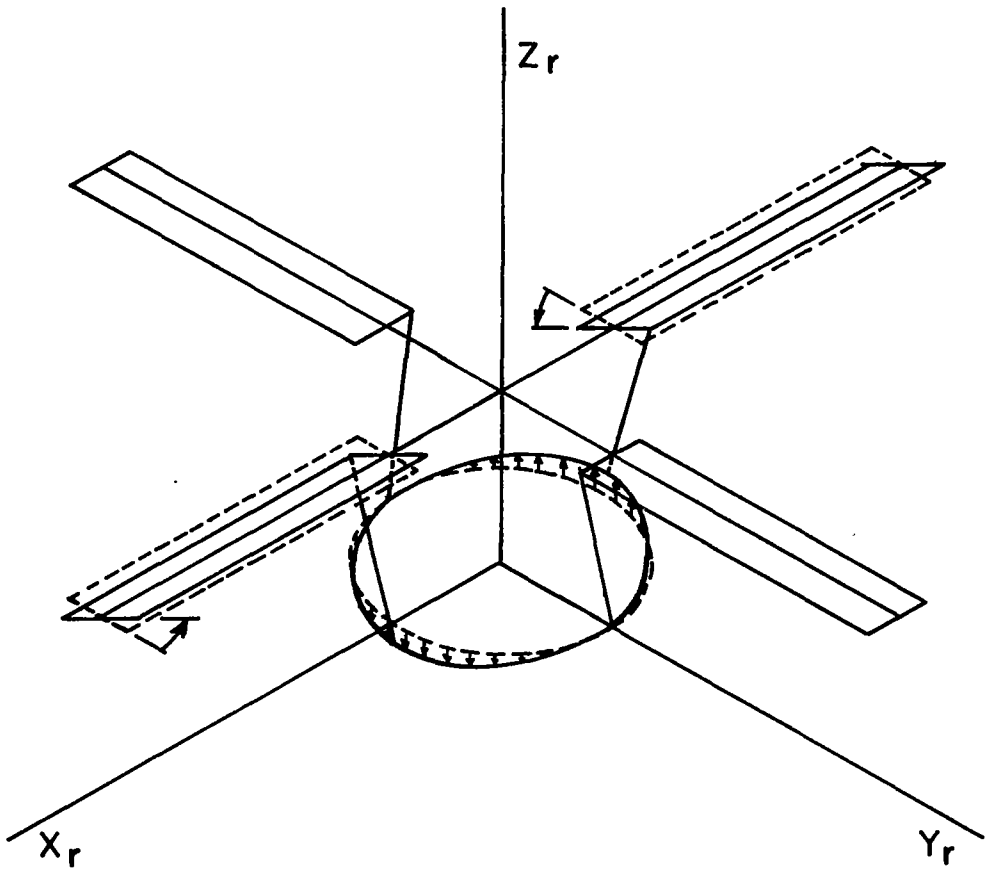

Figure 9. In-phase cyclic mode for simplified OH-6A

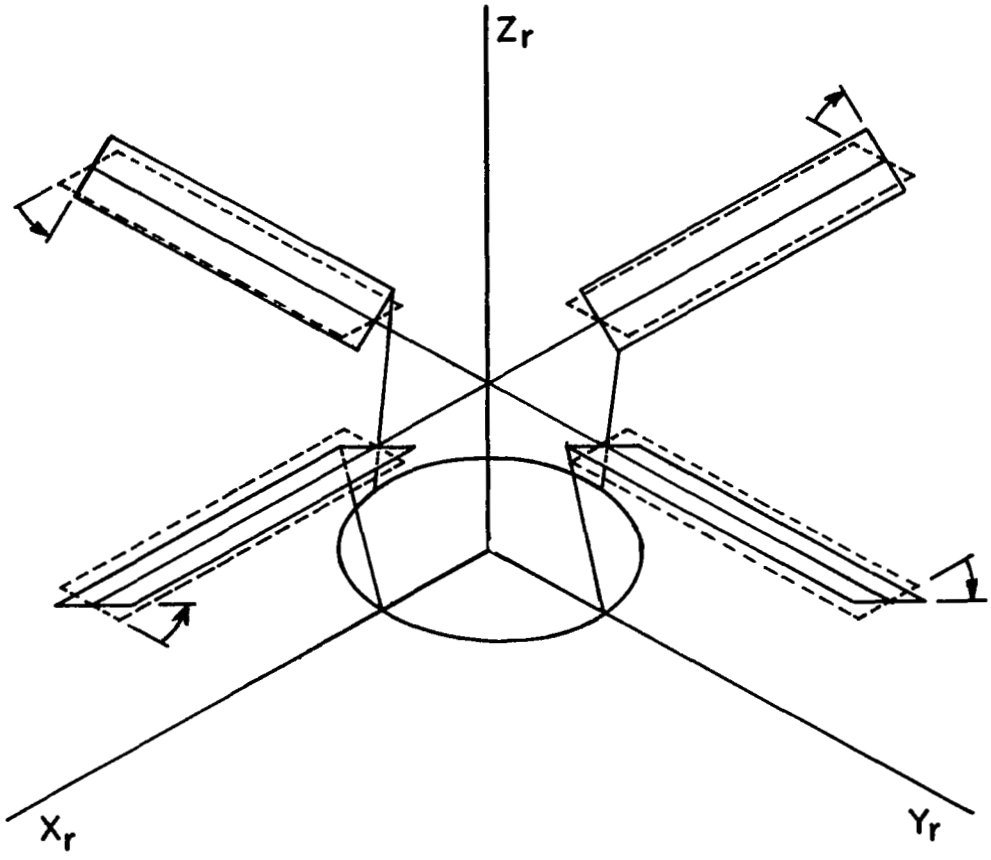

Figure 10. Reactionless mode for simplified OH-6A

TABLE VI

OH-6A FULLY ASYMMETRIC SUPPORTS

	Eigenvalue		Blade Tip Deflections				Blade Root Deflections				Swash-Plate Response in Each Harmonic		
	σ	ω	1	2	3	4	1	2	3	4	$\bar{w}_{-1}$	$\bar{w}_0$	$\bar{w}_1$
T	+.04	115.01	+1.0	-1.0i	-1.0	+1.0i	+.83	-.83i	-.83	+.83i	+.35	0	0
T	-.018	136.2	+1.0	+1.0i	-1.0	-1.0i	+.75	+.75i	-.75	-.75i	0	0	+.269
T	+.096	215.9	+1.0	-1.0	+1.0	-1.0	+.38	-.38	+.38	-.38	0	0	0
T	-.0013	288.7	+1.0	+1.0	+1.0	+1.0	-.02	-.02	-.02	-.02	0	-.15	0
T	-.0018	291.0	+1.0	-1.0i	-1.0	+1.0i	-.032	+.032i	+.032	-.032i	-.15	0	0

It can be seen that in contrast to the cyclic modes the symmetric and reactionless modes do not change significantly from the uniform case of symmetric control stiffness. In particular the lowest forward whirl mode (cyclic) became unstable. Similar sets of results for different values of lateral and longitudinal cyclic stiffnesses were obtained and the effect on the two lower cyclic modes is shown in Table VII. It is clear that the mode that becomes unstable is more unstable with increasing asymmetry.

Swash-plate Flexibility:-The effect of swash-plate flexibility was investigated by accounting for the first bending and torsional mode of the swash-plate using two different sets of swash-plate stiffness. There was little notable effect on the modes investigated except that the unstable reactionless mode became more unstable with increasing flexibility. The effect of swash-plate flexibility on the reactionless mode may be due to either a general sensitivity of that mode to root stiffness or possibly because the increased flexibility of the swash-plate amplifies the non-uniform support stiffness. The unstable reactionless mode, for the fully asymmetric support situation, is shown in Table VIII for three different swash-plate flexibilities.

Effect of Operating Speed.-Some indication of the effect of rotor operating speed on the unstable cyclic mode was gained from results for operating speeds of 40, 45, and 55 rad/sec for a fixed value of support asymmetry. These additional runs were made with a swash-plate support asymmetry described by stiffness pair, J, in Table VII. The cyclic eigenvalues for these operating speeds are presented in Table IX. Note that the mode is stable at operating speeds of 40 and 45 rad/sec, while it is unstable at Ω = 50 and 55 rad/sec. The magnitude of the growth rate indicates that one unstable range of operating speeds begins between 45 and 50 rad/sec and that there may be another unstable range which has an upper boundary slightly below Ω = 40 rad/sec.

Blade Track:-The effect of blade track on the two lowest cyclic modes and the reactionless modes was also investigated. Using the fully asymmetric support stiffness configuration with one blade out of track by one blade thickness the program was used to obtain three eigenvalues. There was very little effect noted except that the reactionless mode became less unstable. Whereas with a balanced blade set the real part of the eigenvalue was .096 rad/sec, the slight blade set asymmetry caused the growth rate to drop to .063 rad/sec.

In summary, the results obtained from the OH-6A study indicate a significant effect from the swash-plate mass and elastic effects on the feathering and torsional modes of such a system. It must be noted that while the blade data used in this study was very detailed and representative of the OH-6A blade, the swash-plate

TABLE VII

EIGENVALUES OF CYCLIC MODES FOR DIFFERING DEGREES OF ASYMMETRY

	Eigenvalue		Blade Tip Deflections				Blade Root Deflections				Swash-Plate Response in Each Harmonic		
	σ	ω	1	2	2	4	1	2	3	4	$\bar{w}_{-1}$	$\bar{w}_0$	$\bar{w}_1$
				forward whirl mode									
A*	-.05	125.7	+1.0	-1.0i	-1.0	+1.0i	+.79	-.79i	-.79	+.79i	+.30	0	0
J	+.0308	123.9	+1.0	-1.0i	-1.0	+1.0i	+.80	-.80i	-.80	+.80i	+.307	0	0
N	+.035	119.8	+1.0	-1.0i	-1.0	$\pm$1.0i	+.86	-.86i	-.86	+.86i	+.322	0	0
R	+.04	115.0	+1.0	-1.0i	-1.0	+1.0i	+.83	-.83i	-.83	+.83i	+.35	0	0
				backward whirl mode									
A	-.011	169.1	+1.0	+1.0i	-1.0	-1.0i	+.70	+.70i	-.70	-.70i	0	0	+.22
G	-.0115	148.6	+1.0	+1.0i	-1.0	-1.0i	+.71	+.71i	-.71	-.71i	0	0	+.226
J	-.0117	147.9	+1.0	+1.0i	-1.0	-1.0i	+.72	+.72i	-.72	-.72i	0	0	+.229
R	-.018	136.2	+1.0	+1.0i	-1.0	-1.0i	+.75	+.75i	-.75	-.75i	0	0	+.269

*Following are combinations of lateral and longitudinal cyclic stiffnesses.

	A	G	J	N	R
Lateral Stiffness	1368.3	1492.7	1566.2	1741.4	2001.5
Longitudinal Stiffness (newton-meters/rad)	1368.3	1243.9	1170.4	995.1	735.0

TABLE VIII

EFFECT ON REACTIONLESS MODE OF SWASH-PLATE FLEXIBILITY

Eigenvalue		Blade Tip Deflections				Blade Root Deflections				Swash-Plate Response in Each Harmonic		
σ	ω	1	2	3	4	1	2	3	4	$\bar{w}_{-1}$	$\bar{w}_0$	$\bar{w}_1$
	Rigid Swash-Plate											
+.096	215.9	+1.0	-1.0	+1.0	-1.0	+.38	-.38	+.38	-.38	0	0	0
	Flexible Swash-Plate											
+.125	215.5	+1.0	-1.0	+1.0	-1.0	+.385	-.385	+.385	+.385	0	0	0
	Flexible Swash-Plate (75% as stiff as previous case)											
+.138	215.36	+1.0	-1.0	+1.0	-1.0	+.385	-.385	+.385	+.385	0	0	0

TABLE IX

EFFECT OF OPERATING SPEED ON UNSTABLE CYCLIC MODE

Eigenvalue		Blade Tip Deflections				Blade Root Deflections				Swash-Plate Response in Each Harmonic		
σ	ω	1	2	3	4	1	2	3	4	$\bar{w}_{-1}$	$\bar{w}_0$	$\bar{w}_1$
Ω = 40 rad/sec												
-.0058	125.4	+1.0	-1.0i	-1.0	+1.0i	+.79	-.79i	-.79	+.79i	+.294	0	0
Ω = 45 rad/sec												
-.011	124.7	+1.0	-1.0i	-1.0	+1.0i	+.796	-.796i	-.796	+.796i	+.301	0	0
Ω = 50 rad/sec												
+.03	123.9	+1.0	-1.0i	-1.0	+1.0i	+.80	-.80i	-.80	+.80i	+.307	0	0
Ω = 55 rad/sec												
+.0138	123.5	+1.0	-1.0i	-1.0	+1.0i	+.81	-.81i	-.81	+.81i	+.317	0	0

mass and elastic properties were arbitrarily assumed. Therefore, the specific numerical results should not be given as much importance as the qualitative effect of the swash-plate.

The effect of blade out-of-track on stability for the OH-6A model was not found to be significant. However, these results may in part be due to the fact that this model had a flap hinge inboard of the pitch bearings.

Studies of the XH-51 Rotor System

Studies of the three-bladed XH-51 representative rotor system were carried out using a set of simplified blade data that was available. Data for the control system stiffness characteristics was obtained from NASA. Explicit data on the swash-plate properties was not available and, therefore, values which seemed reasonable were used. The basic characteristics of this system used are listed in Table X.

This rotor system is unique in that it has a gyro which directly couples the three blades. That is, rather than having the swash-plate connected to the blades through push-pull rods, the swash-plate is connected to the gyro, which in turn is connected to the rotor blades. Since the model used in this study does not presently account for the gyro explicitly, the gyro was simulated by placing a concentrated torsional inertia at the root of each blade. The actual polar moment of inertia of the gyro was 10.1 kilogram-meters^2 and the corresponding inertia placed at the root of each blade was 6.65 kilogram-meters^2. In order to make the simulation as representative as possible, the swash-plate and the push-pull rods connecting the swash-plate to the blades were made rigid.

The initial set of results obtained for the XH-51 system was for the first set of feathering and torsion modes for the case of a balanced blade set. There was very little collective damping in the control system for these calculations. Cyclic damping was as presented in Table X. The results obtained for these conditions are given in Table XI. The six eigenvalues obtained are in two groups of three each clustered around the rotor operating speed (Ω = 37.17 rad/sec) and the cantilever torsion frequency of a single blade (Ω = 265 rad/sec). The large gyro inertia accounts for the natural frequencies being grouped near one-per-rev and near the cantilever torsion frequency. Of those grouped around the operating speed the most marginally stable eigenvalue (3T) has the swash-plate and the gyro whirling backwards at a precession rate of 0.26 rad/sec (viewed from the fixed frame of reference). The other cyclic mode (2T) would result in the gyro swash-plate whirling forward with an apparent precession rate of 74.21 rad/sec. This

TABLE X

BASIC CHARACTERISTICS OF X-51 MODEL

Blade length	5.334	meters
Blade torsional inertia	0.1365	kilogram-meters^2
Blade mass	30.652	kilograms
Swash-plate mass	3.473	kilograms
Gyro polar moment	10.177	kilogram-meters^2
Swash-plate control stiffnesses:		
Lateral	81.418	newton-meters/radian
Longitudinal	81.418	newton-meters/radian
Collective	78.976	newton-meters/radian
Swash-plate control damping:		
Lateral	81.418	newton-meters/rad/sec
Longitudinal	81.418	newton-meters/rad/sec
Collective	0.0	newton-meters/rad/sec

TABLE XI

EIGENVALUES FOR X-51 WITH BALANCED BLADE SET, SMALL COLLECTIVE DAMPING

	Eigenvalue		Blade Tip Deflections			Blade Root Deflections			Swash-Plate Response in Each Harmonic		
	σ	ω	1	2	3	1	2	3	$\bar{w}_{-1}$	$\bar{w}_0$	$\bar{w}_1$
1T	-0.0175	36.94	+1.0	+1.0	+1.0	+1.0003	+1.0003	+1.0003	0	+.500	0
2T	-2.98	37.04	+1.0	-0.50 -0.866i	-0.50 +0.866i	+1.0003	-0.503 +0.864i	-0.497 -0.868i	+.500	0	0
3T	-0.0064	37.33	+1.0	-0.500 +0.866i	-0.500 -0.866i	+0.9998	-0.4999 +0.8659i	-0.4999 -0.8659	0	0	+.499
4T	-0.027	272.42	+1.0	-0.500 -0.866i	-0.500 +0.866i	+0.017	-0.0087 -0.0148i	-0.0084 +0.0149	-.0063	0	0
5T	-5×10^{-6}	272.43	+1.0	+1.0	+1.0	+0.017	+0.017	+0.017	0	-.0063	0
6T	-0.021	272.43	+1.0	-0.500 +0.866i	-0.500 -0.866i	+0.0171	-0.0084 +0.0149i	-0.0086 -0.0147i	0	0	-.0063

mode is much more highly damped, however, and may be more difficult to excite. The remaining mode in the vicinity of the operating speed is a collective mode.

The three eigenvalues grouped at 272 rad/sec all involve very little motion of the swash-plate (gyro). That motion is sufficient, however, to enable the three different modes to exist. Evidently the symmetric "umbrella" mode (5T) is most likely to be seen because of the very low decay rate associated with that mode.

Only a few calculations were performed with one of the blades of the XH-51 system out-of-track. However, the backward whirl mode which was the least stable of the modes near the operating speed, became even less stable with the unbalanced blade set. Table XII contains highlights on the results for the unbalanced blade set.

It should be noted that there is some question as to the meaning of these results in relation to the actual XH-51 due to the fact that the analysis does not account for a gyro explicitly. However, it is believed that the behavior predicted is qualitatively correct. In this regard it should also be noted that this program has proven to be somewhat unique in that it can separate out modes that have almost identical natural frequencies.

CONCLUDING REMARKS

A method of analysis and computer program have been developed for investigating the fully coupled vibration modes and the stability characteristics of a helicopter rotor whose blades are coupled through a flexible, anisotropically mounted swash-plate. The use of a transfer matrix approach combined with the application of the Laplace transform has been shown to be a powerful analytical means of representing the physics of a coupled system of rotor blades. This analysis provides both a basis for solving free vibration and stability problems as well as steady-state forced response and transient response problems. The computer program developed in this study, although specifically developed for studying rotor instabilities, is also well suited as a design tool. It was found to be accurate based upon both the program's ability to predict modes with frequencies close to each other, as well as its capability to adequately satisfy boundary conditions.

To date no known rotor blade dynamic analyses have accounted for coupling with effects of anisotropically-supported flexible swash-plates. Instead, the presence of a pitch control mechanism in rotor blade dynamic analyses has usually been taken into account by introducing an effective torsional spring at the blade root. In this study, however, where the non-uniformities of the swash-plate

TABLE XII

X51 - CASE OF ONE BLADE OUT-OF-TRACK

Eigenvalue		Blade Tip Deflections			Blade Root Deflections			Swash-Plate Response in Each Harmonic		
σ	ω	1	2	3	1	2	3	$\bar{w}_{-1}$	$\bar{w}_0$	$\bar{w}_1$
-2.977	37.02	+1.0	-.519 -.860i	-.486 +.878i	+1.0003	-.5218 -.8583i	-.4833 +.8805i	+.5014	0	0
-0.006	37.32	+1.0	-.589 +.909i	-.564 -.914i	+0.9998	-.5889 +.9087i	-.5640 -.9134i	0	0	+.5257
-0.027	272.43	+1.0	-.495 -.871i	-.506 +.868	+0.0171	-.0086 -.0148i	-.0085 +.0150i	-.0063	0	0
-0.021	272.43	+1.0	-.496 +.860i	-.503 -.864i	+0.0171	-.0084 +.0148i	-.0087 -.0147i	0	0	-.0063

have been accounted for, their resulting effects on rotor blade dynamics have proven to be important. Specifically, it has been found that:

1. Accounting for the swash-plate introduces new modes which are not predicted from a standard single blade analysis.

2. Swash-plate dynamics can also significantly affect modes which are predicted in a single blade analysis.

3. An unstable reactionless mode was found which appeared to be attributable to blade torsion coupling with the first chordwise bending mode and acting together with the lead-lag damper.

4. A forward whirl cyclic mode, which had been stable in the case of uniform supports, became unstable as a small amount of support asymmetry was introduced. Results even showed instability for support asymmetries that were less extreme than actual design values. The growth rate of the instability was found to increase with increasing support asymmetry.

5. It was found that effects of swash-plate mass and support flexibility played a greater role than the contribution of swash-plate flexibility. For example, neglecting the swash-plate mass can cause certain modes to be missed altogether, and as already noted, asymmetry of the support stiffnesses can cause certain modes to become unstable.

6. Modes arising from coupling with the swash-plate mass will not appear in the conventional single-blade analysis. However, an effective spring-mass system could be introduced at the root for the single-blade analysis so as to simulate certain of the modes found in this study. This would require carrying out the coupled analysis first, and in general, using a different effective root impedance for each mode. However, cyclic modes resulting from support asymmetry would be difficult to simulate.

The results obtained in this study should be regarded as qualitative since some of the swash-plate input parameters were arbitrarily assumed due to lack of more specific data. It is believed, however, that the role of the swash-plate control system as an important influence on blade torsional stability and response has been demonstrated. It should be emphasized that the effect of aerodynamics has not been included in this study. This contribution will modify the results obtained herein. However, the study has demonstrated that accounting for non-uniform pitch control dynamics is important for aeroelastic stability and dynamic analyses of rotor systems.

REFERENCES

1. Pestel, E.C. and Leckie, F.A.: Matrix Methods in Elastomechanics. McGraw-Hill Book Co., New York, 1963.